


RESEARCH

Open Access



EZH2 inhibition or genetic ablation suppresses cyst growth in autosomal dominant polycystic kidney disease

Jiayi Lv^{1†}, Bingxue Lan^{2,3†}, Lili Fu^{1†}, Chaoran He³, Wei Zhou⁴, Xi Wang^{5,6}, Chenchen Zhou⁷, Zhiguo Mao^{1*}, Yupeng Chen^{3*}, Changlin Mei^{1*} and Cheng Xue^{1*} 

Abstract

Background Autosomal Dominant Polycystic Kidney Disease (ADPKD) is a prevalent genetic disorder characterized by the formation of renal cysts leading to kidney failure. Despite known genetic underpinnings, the variability in disease progression suggests additional regulatory layers, including epigenetic modifications.

Methods We utilized various ADPKD models, including *Pkd1* and *Ezh2* conditional knockout (*Pkd1*^{delta/delta};*Ezh2*^{delta/delta}) mice, to explore the role of Enhancer of Zeste Homolog 2 (EZH2) in cystogenesis. Pharmacological inhibition of EZH2 was performed using GSK126 or EPZ-6438 across multiple models.

Results EZH2 expression was significantly upregulated in *Pkd1*^{-/-} cells, *Pkd1*^{delta/delta} mice, and human ADPKD kidneys. EZH2 inhibition attenuates cyst development in MDCK cells and a mouse embryonic kidney cyst model. Both *Ezh2* conditional knockout and GSK126 treatment suppressed renal cyst growth and protected renal function in *Pkd1*^{delta/delta} mice. Mechanistically, cAMP/PKA/CREB pathway increased EZH2 expression. EZH2 mediated cystogenesis by enhancing methylation and activation of STAT3, promoting cell cycle through p21 suppression, and stimulating non-phosphorylated β -catenin in Wnt signaling pathway. Additionally, EZH2 enhanced ferroptosis by inhibiting SLC7A11 and GPX4 in ADPKD.

Conclusion Our findings elucidate the pivotal role of EZH2 in promoting renal cyst growth through epigenetic mechanisms and suggest that EZH2 inhibition or ablation may serve as a novel therapeutic approach for managing ADPKD.

[†]Jiayi Lv, Bingxue Lan and Lili Fu contributed equally to this work.

*Correspondence:

Zhiguo Mao
maozhiguo93@163.com
Yupeng Chen
ychen@tmu.edu.cn
Changlin Mei
changlinmei@smmu.edu.cn
Cheng Xue
chengxia1568@126.com

Full list of author information is available at the end of the article



© The Author(s) 2024. **Open Access** This article is licensed under a Creative Commons Attribution-NonCommercial-NoDerivatives 4.0 International License, which permits any non-commercial use, sharing, distribution and reproduction in any medium or format, as long as you give appropriate credit to the original author(s) and the source, provide a link to the Creative Commons licence, and indicate if you modified the licensed material. You do not have permission under this licence to share adapted material derived from this article or parts of it. The images or other third party material in this article are included in the article's Creative Commons licence, unless indicated otherwise in a credit line to the material. If material is not included in the article's Creative Commons licence and your intended use is not permitted by statutory regulation or exceeds the permitted use, you will need to obtain permission directly from the copyright holder. To view a copy of this licence, visit <http://creativecommons.org/licenses/by-nc-nd/4.0/>.

Keywords Polycystic kidney disease, Autosomal dominant, Epigenetics, Enhancer of zeste homolog 2, Ferroptosis, p21

Introduction

Autosomal dominant polycystic kidney disease (ADPKD) is the most common inherited kidney disease and is characterized by progressive enlargement of fluid-filled cysts in both kidneys, often leading to kidney failure [1, 2]. About 85% and 10% of ADPKD patients are affected by mutations of *PKD1* and *PKD2*, which encode polycystin 1 and 2, respectively [1, 3]. Several abnormal signaling pathways have been identified in ADPKD pathogenesis and progression, such as the cAMP, mTOR, JAK-STAT pathways [4, 5]. However, the variability in the severity and progression of ADPKD among individuals with the same genetic mutation suggests that other factors, especially epigenetic modifications, play crucial roles in modulating ADPKD phenotypes.

Epigenetics is a rapidly evolving field that offers new insights into the mechanisms of genetic regulation in ADPKD [6, 7]. Epigenetic mechanisms such as DNA methylation, histone modifications, and non-coding RNAs can influence gene expression levels and have been implicated in the pathogenesis of ADPKD. Studies have shown that mutations in *PKD* genes may result in epigenetic changes that promote renal cyst formation. For instance, *PKD1* mutations increase the expression of various epigenetic regulators, including DNA methyltransferases, histone deacetylases (HDACs), histone methyltransferases, and bromodomain proteins [8].

Targeting these epigenetic modifications, such as inhibiting Sirt1 (a class III HDAC) with nicotinamide, has been found to delay cyst growth and preserve renal function in animal models [9]. HDACs are the most studied epigenetic modifiers in ADPKD [7]. Inhibition of HDACs by pharmaceutical agents reduced the growth of renal cysts [7]. In addition, the epigenetic reader bromodomain-containing protein 4 (BRD4) is up-regulated in renal tissues of *Pkd1* mutant mice [10]. Animal studies showed that inhibition of BRD4 delayed the progression of PKD [10]. SMYD2, a lysine methyltransferase, was increased in renal tissues of *pkd1*-knockout mice and ADPKD patients [11]. SMYD2 has been proven to promote cyst growth via IL-6/STAT3 and TNF- α /NF- κ B signalings in ADPKD [11]. Knockout or inhibition of SMYD2 ameliorated ADPKD progression, indicating that SMYD2 was an epigenetic regulator of ADPKD [11].

Enhancer of Zeste Homolog 2 (EZH2) is a critical component of the Polycomb Repressive Complex 2 (PRC2), functioning primarily as a histone methyltransferase that catalyzes the trimethylation of histone H3 on lysine 27 (H3K27me3), leading to gene silencing [12–14]. Over the years, EZH2 has garnered significant attention due

to its overexpression and/or mutational activation in a wide array of cancers, including hematological malignancies and solid tumors, where it often correlates with aggressive disease, poor prognosis, and resistance to therapy [12, 13]. However, the roles of EZH2 have not been explored in ADPKD. In this study, we investigated expressions, functions, and mechanisms of EZH2 in ADPKD via multiple models in vivo and in vitro. These findings may provide a molecular basis for the use of EZH2 inhibitors to delay cyst growth with the potential for clinical application.

Methods

Animal experiments

Mouse strains and treatments. *Pkd1^{fl/fl}*:CreER positive mice were provided by Professor G. Germino and T. Watnick at Johns Hopkins University School of Medicine [15]. The study was approved by the review board of Second Military Medical University. The *Ezh2^{fl/fl}*:CreER positive mice on a C57BL/6J background were described previously [16]. Tamoxifen-inducible Cre-expressing CAGGCre-ERTM mice (stock no.: 004682) were purchased from the Jackson Laboratory and used in our previous study [17]. These conditional mice were maintained according to local regulations and guidelines. To generate the early-onset ADPKD mouse model, *Pkd1^{fl/fl}*:CreER positive mice were induced by an intraperitoneal injection of tamoxifen (20 mg kg⁻¹ day⁻¹ formulated in corn oil, T5648, Sigma-Aldrich, St. Louis, MO) at postnatal day 10 (P10). To generate the late-onset ADPKD mouse model, *Pkd1^{fl/fl}*:CreER positive mice were given tamoxifen (125 mg kg⁻¹ day⁻¹) on P25 and P28 which resulted in renal cyst formation after two months. In this study, *Pkd1^{fl/fl}* CreER positive mice treated with tamoxifen were defined as *Pkd1^{delta/delta}* mice; *Pkd1^{fl/fl}*:*Ezh2^{fl/fl}* CreER positive mice treated with tamoxifen were defined as *Pkd1^{delta/delta}*:*Ezh2^{delta/delta}* mice; *Pkd1^{fl/fl}*:*Ezh2^{+/+}* CreER positive mice treated with tamoxifen were defined as *Pkd1^{delta/delta}*:*Ezh2^{+/+}* mice; *Pkd1^{+/+}* CreER positive mice treated with tamoxifen were defined as WT mice.

GSK126 is a highly selective, potent EZH2 methyltransferase inhibitor. Both *Pkd1^{delta/delta}* and wild-type *Pkd1^{+/+}* C57/BL6 mice from the same litters were randomly allocated to the following three groups: *Pkd1^{+/+}* control, *Pkd1^{delta/delta}* GSK126, and *Pkd1^{delta/delta}* control (8 mice in each group, male: female=1:1). DMSO (20 μ l/g) and GSK126 (MedChem Express, HY-13470, 30 mg/kg, 3 times/week) were administered to the mice by intraperitoneal injection from P14 to P35 in early-onset *Pkd1^{delta/delta}* mice or from P56 to P150 in late-onset

Pkd1^{delta/delta} mice, respectively. We included mixed male and female mice in all groups. We collected blood samples one day after the last injection and harvested kidneys from P35 (early-onset) and P150 (late-onset) GSK126 and DMSO-treated mice for biochemical and histopathological analyses.

Pkd1^{fl/fl};*Ezh2*^{fl/fl}:CreER positive mice were used to observe the effect of EZH2 on cyst formation and kidney function. The *Ezh2*^{fl/fl} CreER positive mice developed normally and were fertile. *Pkd1*^{fl/fl};*Ezh2*^{fl/fl} CreER positive mice were generated by crossing *Pkd1*^{fl/+};*Ezh2*^{fl/+} CreER positive female mice with *Pkd1*^{fl/+};*Ezh2*^{fl/+} CreER negative male mice. The *Pkd1*^{fl/fl};*Ezh2*^{fl/f} mice and *Pkd1*^{fl/fl};*Ezh2*^{+/+} mice were injected with tamoxifen (50 mg/kg body weight, formulated in corn oil) on P10 to induce *Pkd1* and *Ezh2* gene deletions in the test group ($n=8$, male/female mixed, 1:1). All animals were raised in specific pathogen-free animal facilities according to the protocol approved by the Animal Care Committee of Second Military Medical University, Shanghai, China.

Measurement of the Renal Function. Levels of serum creatinine and blood urea nitrogen (BUN) were measured using a mouse kit (#80350, Crystal Chem, IL) and a BUN colorimetric detection kit (#K024-H5, Arbor Assays, Ann Arbor, MI).

Histology and immunohistochemistry. Paraffin-embedded Sections (2 μm) were used for H&E staining and immunohistochemistry. For EZH2 staining, a rabbit anti-EZH2 antibody (#5246S, 1:50, CST) was used. Ki-67 was stained with anti-Ki-67 (#ab15580, 1:100; Abcam). Images were analyzed via ip 6.0 with Panoramic 250 (3D HISTECH). The ImageJ software was used to quantify the percentage of positively stained areas in immunohistochemistry samples. The cyst index was assessed by morphometry using the point counting method as described previously [18]. The proliferation index analysis was measured via the ratio of Ki-67 positive nuclei to the total number of nuclei which was calculated as a percentage. The numbers of positive and total nuclei were counted (>1000 nuclei for each kidney) using Image Pro-Plus (version 6.0).

XCT (SLC7A11) Detection: Sections were deparaffinized, rehydrated, and incubated with an anti-SLC7A11 antibody (Affinity DF12509, 1:50) overnight at 4 °C. After washing, sections were incubated with HRP-conjugated secondary antibodies and visualized using DAB substrate. Counterstaining was performed with hematoxylin. Positive staining for SLC7A11 was quantified using ImageJ software. **4-Hydroxynonenal (4HNE) Staining:** Sections were deparaffinized, rehydrated, and incubated with an anti-4HNE antibody (Abcam ab48506, 1:25) overnight at 4 °C. After washing, sections were incubated with HRP-conjugated secondary antibodies and visualized using DAB substrate. Counterstaining was performed

with hematoxylin. Positive staining was quantified using ImageJ software. **Prussian Blue Staining:** Sections were deparaffinized, rehydrated, and stained with Prussian Blue stain (Sigma-Aldrich) to detect iron ions for 30 min. Sections were then counterstained with nuclear fast red for 5 min. Iron deposits were visualized and quantified using a light microscope and ImageJ software.

Zebrafish model

Zebrafish (TAB, Tubigen) were raised according to standard protocols in Prof. Ying Cao's laboratory at Shanghai Tongji University. Human EZH2 mRNA (200 pg) was injected into embryos at the one to two-cell stage, as described before [19]. Zebrafish protein was harvested for Western blot analysis. EZH2 mRNA was injected into zebrafish larvae, and pronephic cysts were observed on 3 days post-fertilization from the shield stage. The average percentage of embryos with kidney cysts from 3 independent experiments. 20 embryos were examined in each experiment.

Embryonic kidney cyst model

ICR mouse embryonic kidneys (E13.5) were harvested and placed on 0.4 μm cell culture inserts (Merck Millipore, Billerica, MA, USA). The lower chambers were filled with DMEM/F-12 supplemented with 10 mM HEPES (Sigma H3375), 2 mM L-glutamine (Sigma G7513), 25 ng/ml of prostaglandin E1 (Sigma P5515), 1/100 insulin-transferrin-selenium (Life 41400-045), 32 pg/ml of T3 (Sigma T5516), 1/40 penicillin/streptomycin (Life 15140-122) and 100 μM 8-Br-cAMP (Sigma B5386). The medium was replaced every 12 h. The kidneys were photographed every 2 days. Embryonic kidneys were sectioned and cyst size was calculated on slides.

Human kidney samples

Kidney tissue samples from anonymous ADPKD patients and normal controls were obtained from Changzheng Hospital. The control samples were collected from non-cancerous renal tissue located more than 5 cm away from the tumor lesions in patients undergoing nephrectomy for renal cell carcinoma [20]. Renal cortex tissues surrounding cysts were obtained from ADPKD patients who underwent nephrectomy. All tissues were devoid of contamination and stored in liquid nitrogen before further experiments. Informed consent was obtained from all subjects. The study was approved by the ethics review board of Changzheng Hospital (CZ2018-0619). The study abided by the Declaration of Helsinki principles.

In vitro experiments

Cell Cultures. *Pkd1*^{-/-} (PN24) and *Pkd1*^{+/-} cells (PH2) were obtained from Prof. Stefan Somlo (Yale University, New Haven, CT) [21]. Human immortalized renal cyst

epithelial cells (WT9-12) were kindly provided by Prof. Jing Zhou (Harvard University, Boston, MA, USA), and were cultured as described previously [22]. OX161 cells were human ADPKD cystic lining epithelial cells kindly provided by Prof. Albert CM Ong (Sheffield Kidney Institute, Division of Clinical Sciences, University of Sheffield, UK). *Pkd1* mutant cells and WT9-12 cells were treated with various concentrations of GSK126 for 24 h, 48 h, or more. Human renal tubular epithelial cells (UCL93 and RC7EC) were used as control groups for OX161 and WT9-12 cells, respectively. Reagents used 8-Br-cAMP (Sigma B5386), forskolin (Selleck No.S2449), PKA inhibitor H89 (Selleck No.S1582), and cAMP antagonist Rp-camp (Sigma A165).

siRNA and plasmids. Cells were transfected using Lipo2000 (Lipofectamine®, Invitrogen, Carlsbad, CA, USA) according to the manufacturer's instructions 48 h before protein extraction. EZH2 siRNA (#SC-35312, Santa Cruz), CREB siRNA (#SC-29281, Santa Cruz), and plasmid (Addgene: CMV500 A-CREB, #33371) were used according to the manufacturer's protocol. The HA-tagged EZH2 plasmid was constructed into the pCMVHA vector (Addgene plasmid # 24230).

MTT assays. Cell proliferation was measured via an MTT kit (Sigma-Aldrich) according to the manufacturer's instructions.

Madin-Darby Canine Kidney Cell 3D Culture. Type I Madin-Darby canine kidney (MDCK) cells were cultured in DMEM/F-12 medium (Biological Industries) supplemented with 10% FBS (Biological Industries) and incubated in a humidified incubator at 37°C with 5% CO₂. For 3D culture, MDCK cells were first resuspended in MEM containing 10 mM HEPES, 2.79 mg/ml collagen I (Pure-Col), and 27 mM NaHCO₃ and incubated at 37°C for 90 minutes. Then, DMEM/F12 medium supplemented with 10% FBS and 10 μM forskolin was added to the cells, and spheroid formation was visible after 4 days. The established spheroids (day 4) were treated with GSK126 or EPZ-6438 for another eight days in the presence of 10 μM FSK. For the EZH2 knockdown experiments, we first generated an MDCK cell line that stably expressed Cas9 (MDCK-Cas9). MDCK-Cas9 cells were infected with lentiviruses carrying control or EZH2 sgRNA for 48 hours, followed by puromycin selection for another 48 hours to achieve ideal knockdown efficiencies. The sgRNA sequence targeting exon 1 of EZH2 was as follows: forward 5'-CACCGGCAGCTCAAGAGGTTTCAGGC-3'; reverse 5'-AAACGCCTGAACCTCTTGAGCTGCC-3'. Then, the cells (day 0) were subjected to 3D culture in the presence of 10 μM forskolin. Micrographs of the same spheroids were taken on days 4, 6, 8, 10, and 12. The spheroid numbers and diameters were measured on day 12 using the NIH ImageJ software.

Real-time PCR. Total RNA was extracted using the RNase mini kit (Invitrogen, Carlsbad, CA, USA) and reverse-transcribed. The primer sequences were listed in Supplement 1. Real-time PCR was performed using the SYBR Green PCR Master Mix (Toyobo, Osaka, Japan) and a Rotor-Gene-3000 A Real-Time PCR System (Corbett, Sydney, Australia) according to the manufacturer's protocols. The results are given as relative EZH2 expression normalized to GAPDH expression. The relative amount of mRNA compared with the internal control was calculated by 2^{-ΔΔCT} method: $\Delta\text{CT} = \Delta\text{CT}_{\text{experimental}} - \Delta\text{CT}_{\text{control}}$.

Western Blotting Analyses. Tissue or cell lysates were prepared in RIPA buffer (50 mM Tris HCl, 1 mM EDTA, 150 mM NaCl, 1% Triton, 2% sodium dodecyl sulfate (SDS), and phosphatase and protease inhibitors), and clarified by centrifugation. Equal amounts of protein ran on SDS-polyacrylamide gels, transferred to polyvinylidene difluoride membranes, blocked in 3% bovine serum albumin, and incubated with the primary antibodies. Then appropriate secondary antibodies were used before development with an enhanced chemiluminescence reagent. The primary antibodies were as follows: anti-EZH2 (#5246, 1:1000, CST), anti-STAT3 (#SC-8019, 1:100, Santa CRUZ), anti-p-stat3 (#af3294, 1:1000, Affinity), anti-methylated lysine antibody (ab23366, 1:1000, Abcam), anti-tri-methyl-histone H3 (Lys27) (#07-449, 1:1000, Millipore), Phospho-CREB antibody (AB_2536825, Invitrogen), β-Catenin antibody (D10A8, cst8480, Cell Signaling), Non-phospho (Active) β-Catenin (Ser33/37/Thr41) antibody (CST8814, 1:1000, Cell Signaling), P21 antibody (CST2947, 1:1000, Cell Signaling), GPX-4 antibody (abcam ab125066 1:1000), SLC7A11 antibody (CST12691, 1:500), ACSL4 antibody (Abcam ab155282 1:10000).

Immunoprecipitation Assay. Precleared lysates were used for immunoprecipitation with antibodies against EZH2 or STAT3 after overnight incubation at 4°C and subsequently pulled down using protein A or G agarose/Sepharose beads. The complexes were resolved on SDS-PAGE for Western blotting analysis.

RNA sequencing

The Kidney Interactive Transcriptomics (<https://humphreyslab.com/SingleCell/>) provided a snRNA+scATAC-seq analysis for comparing EZH2 expression levels in ADKD patients and healthy groups [23]. Eight human ADPKD kidneys and five control kidneys were analyzed with snRNA-seq (62,073 nuclei from ADPKD and 40,637 nuclei from control kidneys) and snATAC-seq (17,365 nuclei for ADPKD and 33,621 nuclei for control) by 10X Genomics Chromium Single Cell [24].

Total RNA was collected from WT9-12 cells and WT9-12+EZH2 siRNA cells with TRIzol reagent (Life

Technologies). DJ Group (Shanghai, China) was responsible for RNA sequencing and data processing. To identify differentially expressed genes (DEGs), we used R studio (DESeq2, $\lg|FC| > 2$, $FDR < 0.05$). DEGs were used to create a volcano map and analyzed using KEGG. $P < 0.05$ were considered significant. RNAseq raw data was shown in https://1drv.ms/f/c/cff9170848857f88/EjzEDoMuy49Bi_lsWWmSG_UBloAf_SfyipHahLVmUBLCPg?e=k2Ez2s.

Statistical analyses

Statistical analyses were performed with an unpaired *t*-test or one-way or two-way ANOVA with the Turkey post hoc test using GraphPad Prism version 9.0 (GraphPad, San Diego, CA, USA). All data are expressed as the mean \pm SD, and $P < 0.05$ was considered statistically significant.

Results

EZH2 expression is upregulated in vivo and in vitro in ADPKD

SnRNA-seq data showed that EZH2 had higher levels in ADPKD kidneys than controls, particularly in the proximal tubules, front-row proximal tubular cells, ascending thin limb, thick ascending limb, type B intercalated cell of collecting duct, leukocytes, and endothelial cells (Fig. 1A, B). Then we found that EZH2 mRNA was up-regulated in *Pkd1*^{-/-} cells vs. *Pkd1*^{+/-} cells, WT9-12 cells vs. RCTEC, *Pkd1*^{delta/delta} mice kidneys vs. *Pkd1*^{+/+} mice kidneys, and human ADPKD kidneys vs. normal control kidneys, respectively (Fig. 1C). Western blot analysis indicated that the protein expression of EZH2 and its downstream substrate H3K27me3 were both upregulated in *Pkd1*^{-/-} cells compared with *Pkd1*^{+/-} cells, WT9-12 cells vs. RCTEC, *Pkd1*^{delta/delta} mice kidneys vs. *Pkd1*^{+/+} mice kidneys at P25, and human ADPKD kidneys vs. normal control kidneys, respectively (Fig. 1D-K). Immunohistochemistry analysis indicated that EZH2 and H3K27me3 expression was increased and localized to cyst lining epithelial cells and renal tubular epithelial cells in *Pkd1*^{delta/delta} mice kidneys compared with *Pkd1*^{+/+} mice kidneys (Fig. 2A, B), and human ADPKD kidneys vs. normal control kidneys, respectively (Fig. 2C, D). Negative control DAB IHC stains were shown in Supplement 2.

PKD gene mutation up-regulates EZH2 expression through cAMP pathway in cystic epithelial cells

As cAMP pathway is the most important pathway activated by *Pkd1* mutation to promote cyst growth [5], we tested whether cAMP/PKA/CREB pathway was the upstream of EZH2 in ADPKD. Two cAMP agonists, forskolin (5 to 20 μ M) or 8-Br-cAMP (75 to 150 μ M), dose-dependently increased EZH2 and H3K27me3 protein expression in WT9-12 cells (Fig. 3A, B). And vice

versa, PKA inhibitor H89 and cAMP antagonist Rp-camp reduced protein levels of p-CREB, EZH2, and H3K27me3 in WT9-12 cells dose-dependently from 5 to 50 μ M or from 50 to 200 mM, respectively (Fig. 3C, D). Moreover, CREB siRNA reduced p-CREB, EZH2, and H3K27me3 protein levels. Vice versa, overexpression of human CREB plasmids resulted in increased phosphorylation of CREB, EZH2 expression, and H3K27me3 protein levels in WT9-12 cells (Fig. 3E, F). Figure 3G-L showed related quantitative Western blot bar graphs.

EZH2 inhibition attenuates cystogenesis of MDCK cells

To evaluate the effects of EZH2 inhibition on cystogenesis, an established in vitro 3D-MDCK spheroid cell model was treated with several reagents. Treatment with the cAMP agonist forskolin-induced spheroid formation in MDCK cells grown in collagen gels for 4 days. Treatment with GSK126 (Fig. 4A, B) dose-dependently diminished spheroid enlargement. GSK126 had little or no effect on the total number of established spheroids, indicating that exposure was marginally toxic to MDCK cells (Fig. 4C). EPZ-6438 also dose-dependently diminished spheroid enlargement (Fig. 4D, E) with no effect on the total number of established spheroids (Fig. 4F). Furthermore, we applied CRISPR/Cas9-mediated gene editing to evaluate the effect of EZH2 knockdown. As shown in Fig. 4G-I, EZH2 silencing dramatically reduced spheroid diameters and also significantly reduced spheroid numbers. The efficiency of EZH2 knockdown was confirmed by Western blotting (Fig. 4J).

EZH2 inhibition suppresses cyst development in an embryonic kidney cyst model

To examine the role of EZH2 in cystogenesis, we first analyzed the effects of pharmacological inhibition of EZH2 in cyst formation using a mouse embryonic kidney cyst model [25]. The embryonic kidneys were dissected from CD1 mice at embryonic day 13.5 and grew over 6 days under basal culture conditions. Treatment with 8-Br-cAMP (100 μ M) induced tubule dilation and cyst formation. Cystogenesis was measured by quantifying the fractional cyst area using morphometric analyses. As shown in Fig. 5A and B, GSK126 inhibited cystogenesis in mouse embryonic kidney explants in a dose-dependent manner. To further confirm the anti-cystic effect of EZH2 inhibition, we examined cyst formation with another potent EZH2 inhibitor, EPZ-6438. Consistent with GSK126, EPZ-6438 also inhibited cyst enlargement ex vivo in a dose-dependent manner (Fig. 5C and D).

EZH2 over-expression induces cyst growth in Zebrafish

Human EZH2 protein was exogenously expressed in Zebrafish by injecting *Ezh2* mRNA. 12% of the injected embryos exhibited pronephic cysts on 3 days post

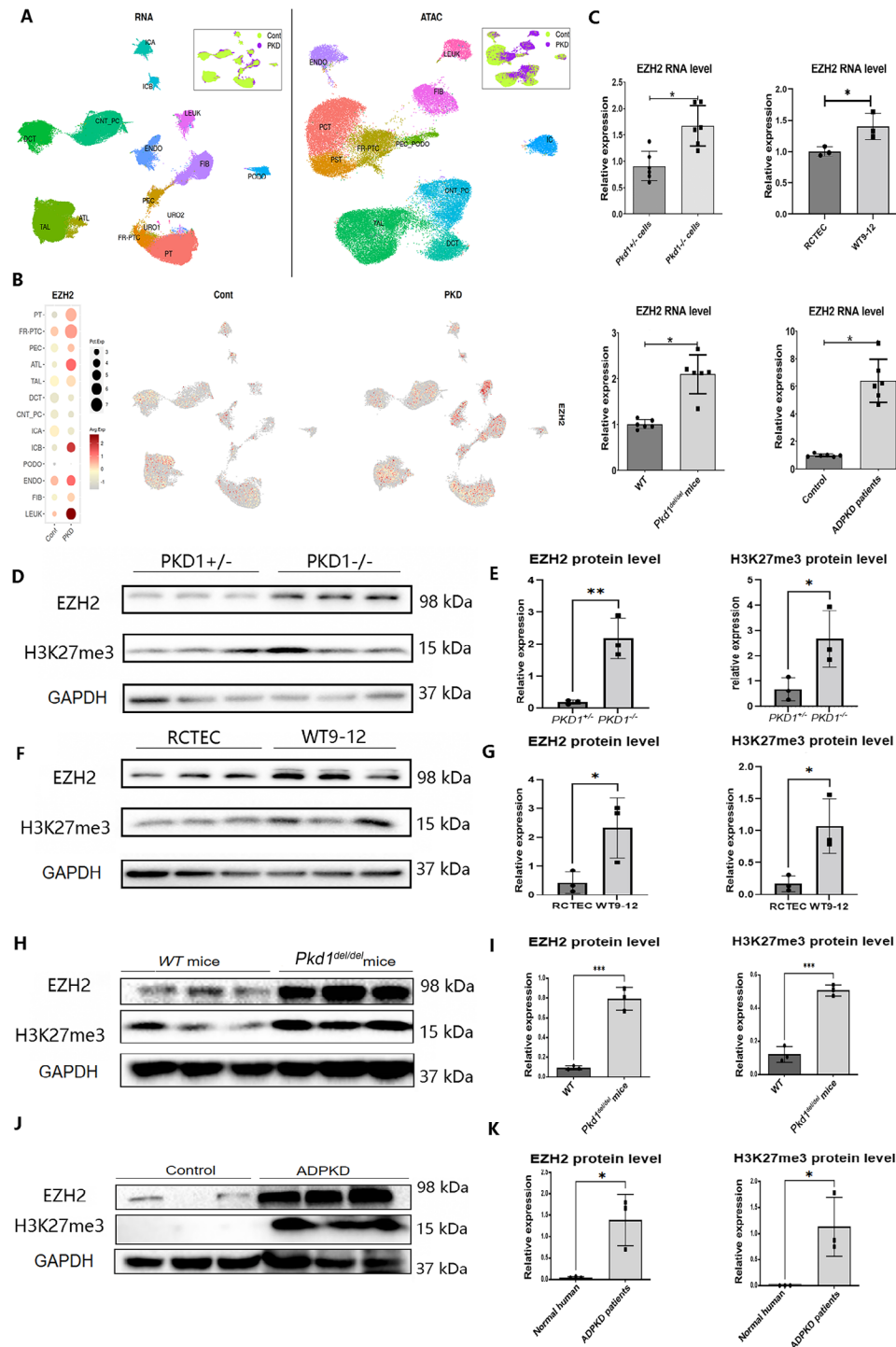


Fig. 1 Increased expression of EZH2 in ADPKD. **(A)** Left: UMAP plot of integrated snRNA-seq dataset with annotation by cell type and disease condition. Right: UMAP plot from an integrated snATAC-seq dataset with gene activity-based cell-type assignments and disease condition. PT: proximal tubules, FR-PTC: Front-row proximal tubular cells, PEC: Parietal Epithelial Cells, ATL: ascending thin limb, TAL: Thick ascending limb, FIB: Fibroblasts, ICB: Type B intercalated cell of collecting duct, LEU: Leukocytes, DCT: Distal Convolved Tubule, CNT-PC: Connecting Tubule Principal Cells, and ENDO: Endothelial cells. **(B)** SnRNA-seq showed EZH2 mRNA levels in different cell types between ADPKD kidneys and controls. **(C)** Quantitative RT-PCR analysis of relative EZH2 mRNA expression in *Pkd1*^{-/-} cells vs. *Pkd1*^{+/+} cells, WT9-12 cells vs. RCTEC, *Pkd1*^{delta/delta} mice kidneys vs. *Pkd1*^{+/+} mice kidneys at P25, and human ADPKD kidneys vs. control, *N* = 6 respectively. **(D, E)** Western blotting of EZH2 and methylated H3K27 (H3K27me3) expression in *Pkd1*^{+/+} cells and *Pkd1*^{-/-} cells (*N* = 3 respectively). **(F, G)** Western blotting of EZH2 and H3K27me3 expression in RCTEC cells vs. WT9-12 cells. **(H, I)** EZH2 and H3K27me3 protein expression in kidney tissues from *Pkd1*^{+/+} vs. *Pkd1*^{delta/delta} mice. **(J, K)** EZH2 and H3K27me3 protein expression in control and human ADPKD kidneys. Statistical analyses were performed with an unpaired t-test or one-way ANOVA with the Turkey post hoc test. **P* < 0.05, ***P* < 0.01, ****P* < 0.001

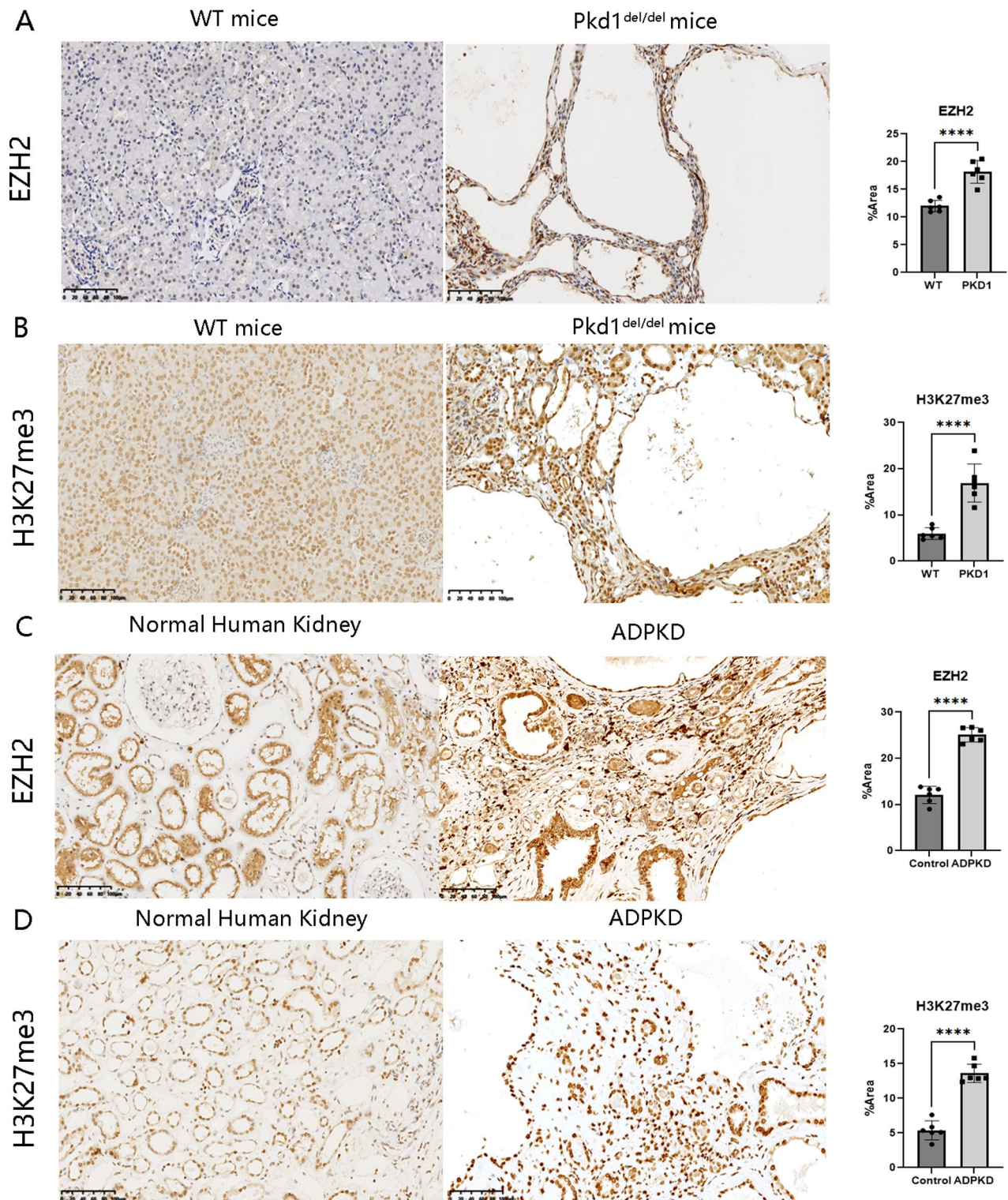


Fig. 2 Immunohistochemistry analysis of EZH2 and H3K27me3 in vivo. **(A and B)** Immunohistochemistry analysis indicated that EZH2 and H3K27me3 expression was increased in cyst lining epithelia and renal tubular epithelial cells in *Pkd1*^{delta/delta} mice kidneys compared with *Pkd1*^{+/+} mice kidneys, $N=6$ respectively. Scale bar: 100 μ m. **(C and D)** EZH2 and H3K27me3 expression was increased in cyst lining epithelia and renal tubular epithelial cells in human ADPKD kidneys compared with normal control kidneys. Statistical analyses were performed with an unpaired t-test. **** $P < 0.0001$

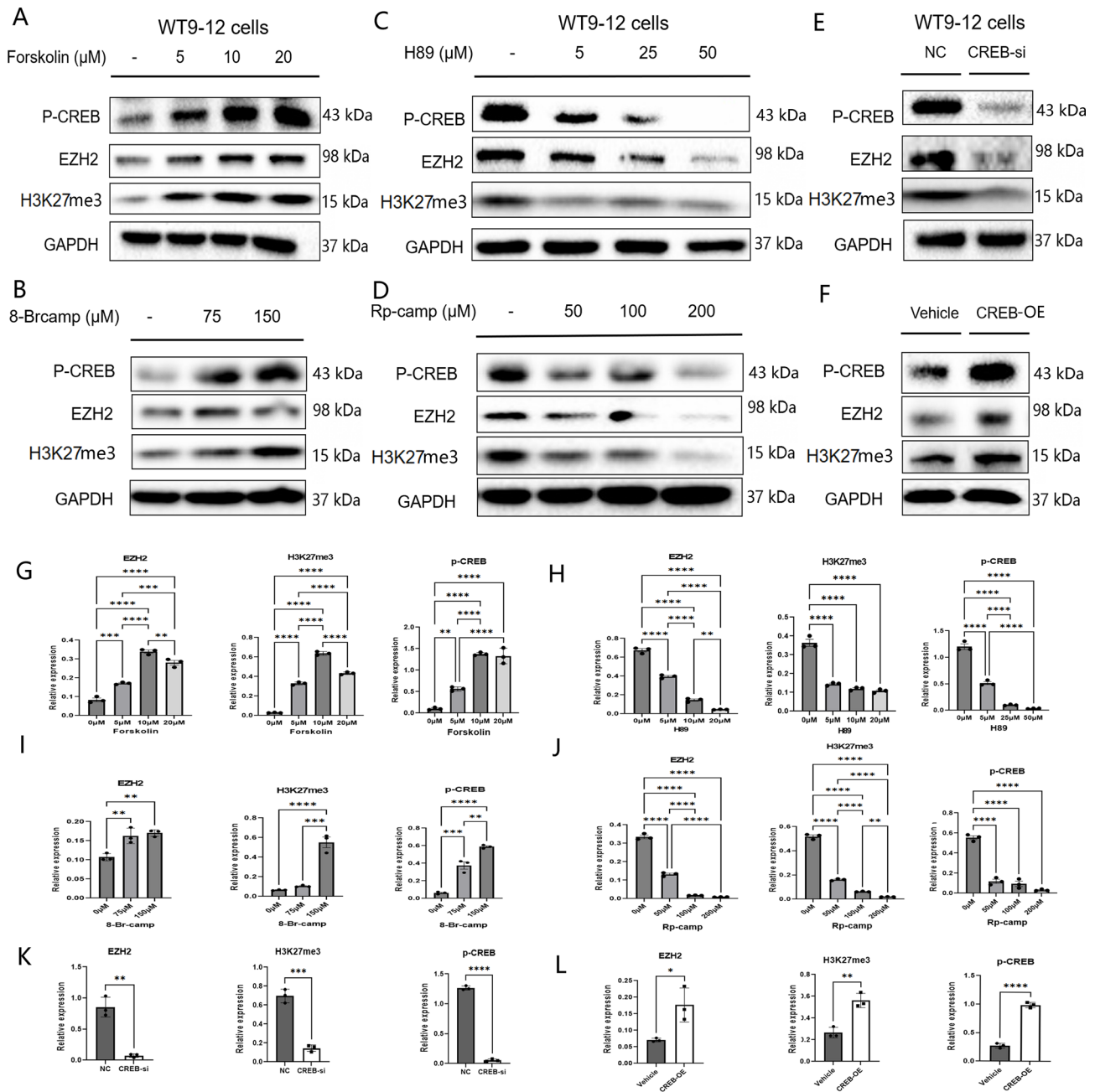


Fig. 3 cAMP/PKA/CREB signaling increased EZH2 expression in cystic epithelial cells. WT9-12 cells were treated with two cAMP agonists forskolin (**A** and **G**) and 8-Br-cAMP (**B** and **I**), PKA inhibitor H89 (**C** and **H**), cAMP antagonist Rp-camp (**D** and **J**), or transfected with CREB siRNA (**E** and **K**) or CREB plasmids (**F** and **L**). The expressions of EZH2, phosphorylation of CREB, and H3K27me3 were evaluated by Western blot, $N=3$ respectively. Statistical analyses were performed with one-way ANOVA with the Turkey post hoc test. * $P<0.05$, ** $P<0.01$, *** $P<0.001$, **** $P<0.0001$

fertilization and heart edema was observed (Fig. 5E and F). Western analysis showed that EZH2 was over-expressed on day 3 after *Ezh2* mRNA injection (Fig. 5G). Meanwhile, EZH2 expression and H3K27me3 levels were not changed in *Ezh2* failed EZH2 injection group. Variability in zebrafish responses occurred due to multiple factors such as injection efficiency and embryo health.

Ezh2 and *Pkd1* double conditional knockout suppresses renal cyst growth

To investigate the functional role of EZH2 in vivo, we generated *Pkd1* and *Ezh2* double conditional knockout *Pkd1*^{delta/delta}.*Ezh2*^{delta/delta} mice (Fig. 6A). We found that cyst index was significantly reduced by 30.3% ($P<0.001$) in *Pkd1*^{delta/delta}.*Ezh2*^{delta/delta} mice at P25 compared with age-matched *Pkd1*^{delta/delta}.*Ezh2*^{+/+} mice (Fig. 6B and H). Total image scanning results were shown in Fig. 6C and

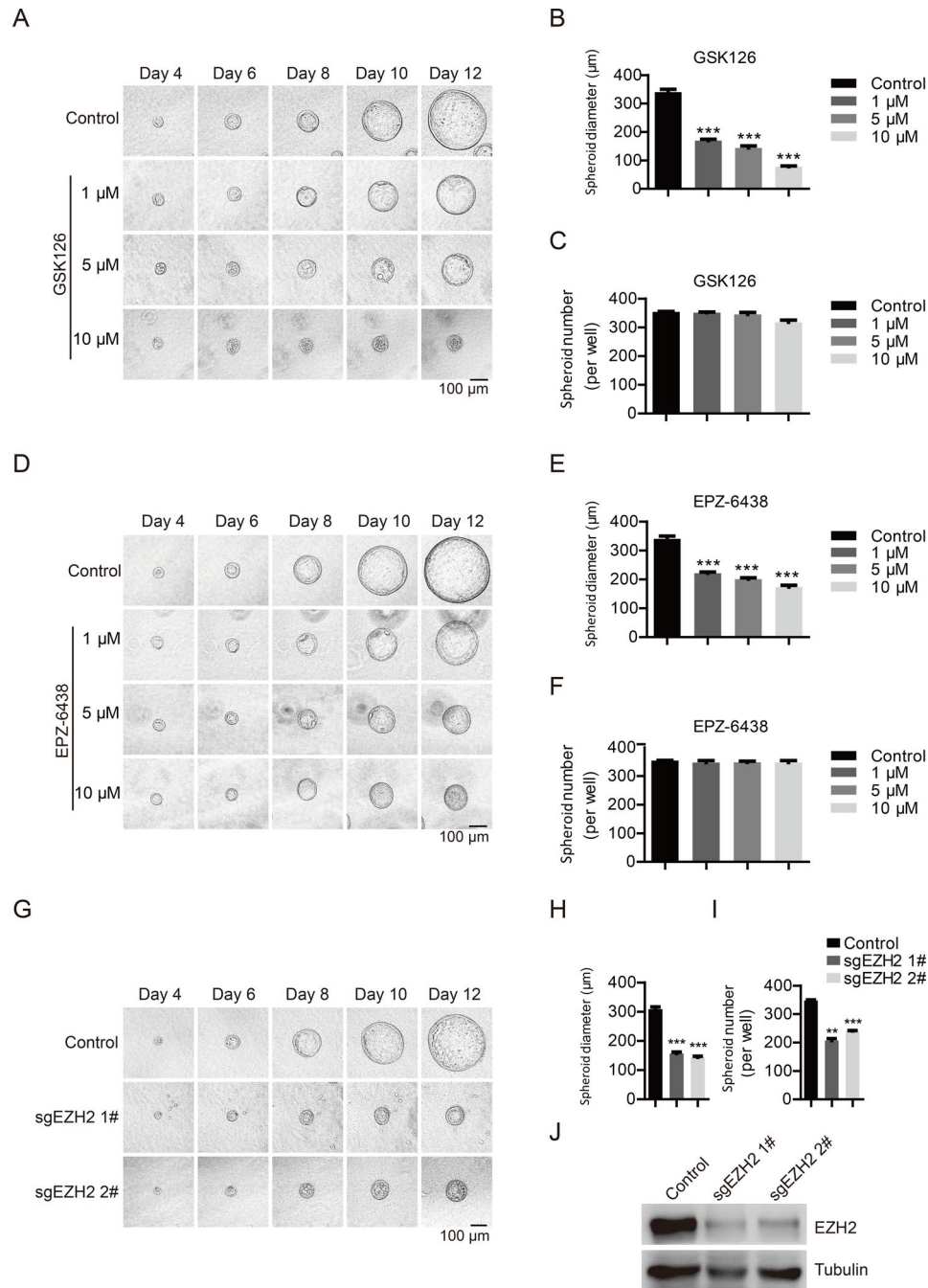


Fig. 4 EZH2 inhibition attenuates cystogenesis in MDCK spheroid cell model. (**A** and **D**) MDCK cells were grown in collagen gels in the presence of 10 μM forskolin. Cells were treated with the indicated doses of GSK126 (**A**) or EPZ-6438 (**D**) from day 4. Micrographs were taken at the indicated time points. Spheroid diameters (**B** and **E**) and spheroid numbers (**C** and **F**) from the indicated groups were counted on day 12. (**G**) MDCK-Cas9 cells infected with lentiviruses carrying control or EZH2 sgRNA were grown in collagen gels in the presence of 10 μM FSK. Micrographs were taken at the indicated time points. (**H** and **I**) Spheroid diameters (**H**) and spheroid numbers (**I**) from the indicated groups were counted on day 12. (**J**) Immunoblotting analysis of EZH2 expression in MDCK-Cas9 cells infected with lentiviruses carrying EZH2-sgRNA or control-sgRNA. Data are represented as the mean \pm SEM. Statistical analyses were performed with one-way ANOVA with the Turkey post hoc test. * $P < 0.05$, ** $P < 0.01$, *** $P < 0.001$

Supplement 3. Two-kidney/total body weight (2KW/TBW) ratio in the *Pkd1*^{delta/delta}.*Ezh2*^{delta/delta} mice was significantly lower than that in the *Pkd1*^{delta/delta}.*Ezh2*^{+/+} mice by 57% ($P < 0.01$) (Fig. 6F). The BUN and serum creatinine levels were elevated in the *Pkd1*^{delta/delta}.*Ezh2*^{+/+}

mice at P25. EZH2 ablation in the *Pkd1*^{delta/delta} mice also significantly decreased the BUN and serum creatinine levels by 58% and 70%, respectively, which indicated that renal function was significantly improved (Fig. 6D and E). Survival rates were not statistically different in P25

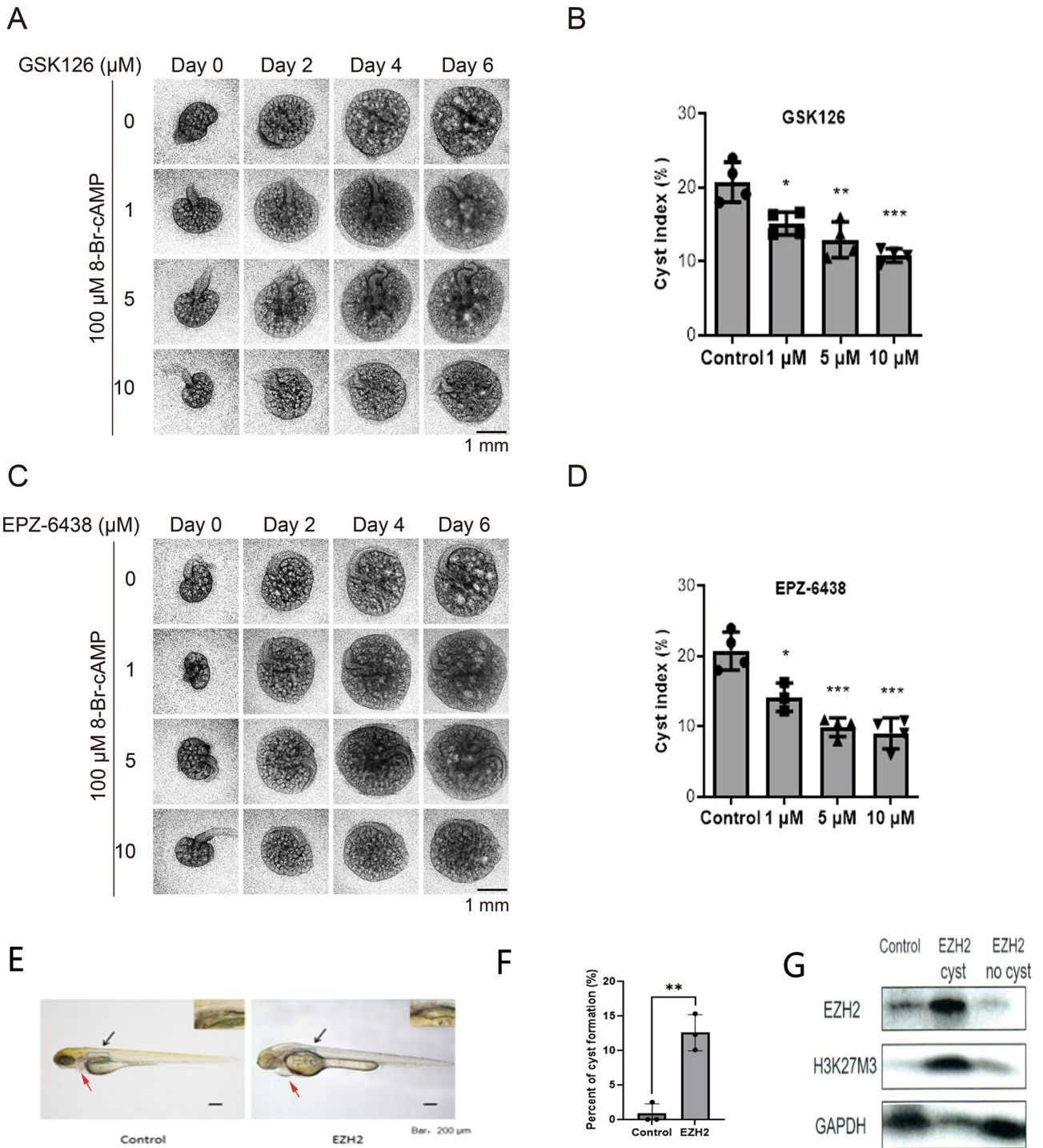


Fig. 5 EZH2 inhibition suppresses cyst formation in embryonic kidney explants while EZH2 over-expression induces cyst growth in Zebrafish. **(A and C)** Mouse embryonic kidneys (E13.5) cultured in the presence of 8-Br-cAMP (100 μM) were treated with the indicated doses of GSK126 **(A)** and EPZ-6438 **(C)** for 6 days, $N=4$ respectively. Micrographs were taken at the indicated time points. **(B and D)** The percentage of the cystic area relative to the total kidney area was measured on day 6. **(E)** Exogenous expression of human EZH2 induced cyst growth in Zebrafishes. The Zebrafish in the control group have no renal cysts, and the general phenotype is normal. The black arrows indicated pronephric cysts, while the red arrows pointed to pericardial cysts. The inset in the top right corner shows an enlarged view of the area marked by the black arrow. EZH2 overexpression Zebrafish group had obvious pronephric cysts and mild pericardial edema. **(F)** The proportion of prerenal cysts in zebrafish in control group and EZH2 overexpression group. **(G)** Western blotting showed protein expressions of EZH2 and H3K27me3 of zebrafish in the control group, EZH2 overexpression with renal cyst group, and failed EZH2 injection group, $N=3$ respectively. Statistical analyses were performed with one-way ANOVA with the Turkey post hoc test. * $P < 0.05$, ** $P < 0.01$, *** $P < 0.001$

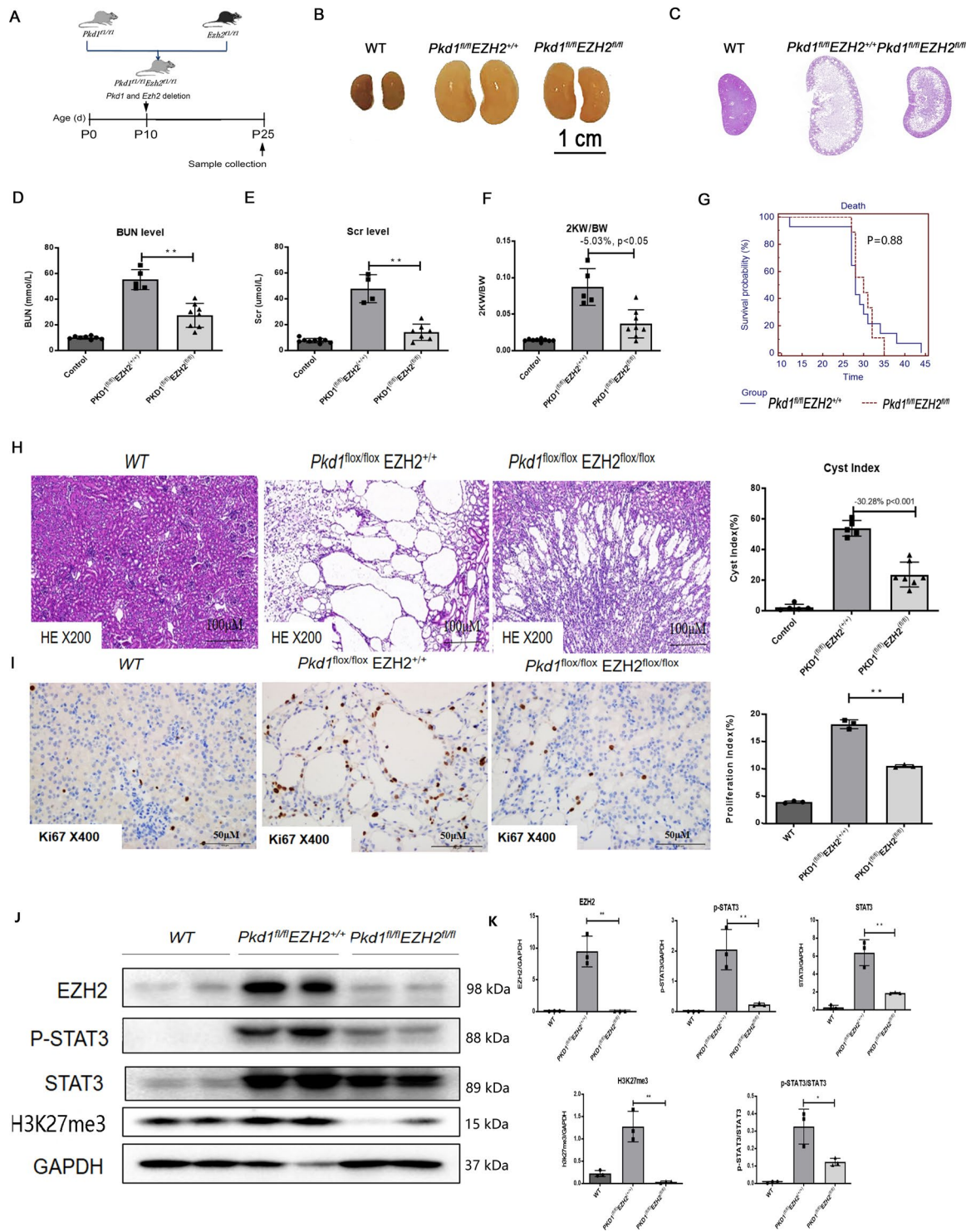


Fig. 6 Double conditional knockout of *Pkd1* and *Ezh2* suppresses cyst growth in *Pkd1^{delta/delta}* mice. **(A)** Schedule of the induction of *Pkd1* and *Ezh2* conditional knockout mice ($n = 8$ each group). **(B)** Representative kidneys from *Pkd1^{+/-}.Ezh2^{+/-}* mice, *Pkd1^{flox/flox}.Ezh2^{+/-}* mice (*Pkd1^{flox/flox}.Ezh2^{+/-}* mice), and *Pkd1^{delta/delta}.Ezh2^{delta/delta}* mice (*Pkd1^{flox/flox}.Ezh2^{fl/fl}* mice). Scale bar: 1 cm. **(C)** Total image scanning of histological kidneys on P25 from the three groups mentioned above. **(D and E)** BUN and creatinine levels were significantly decreased in P25 serum from *Pkd1^{delta/delta}.Ezh2^{delta/delta}* mice compared with *Pkd1^{delta/delta}.Ezh2^{+/-}* mice. **(F)** 2KW/TBW ratios. **(G)** Survival rates were not statistically different in P25 *Pkd1^{delta/delta}.Ezh2^{delta/delta}* mice vs. *Pkd1^{delta/delta}.Ezh2^{+/-}* mice. **(H)** The cyst index. **(I)** Cell proliferation detected via Ki67 staining. **(J and K)** Western blotting of EZH2, p-STAT3, STAT3, and H3K27me3 expression from wild type mice, *Pkd1^{delta/delta}.Ezh2^{+/-}* mice, and *Pkd1^{delta/delta}.Ezh2^{delta/delta}* mice in P25. Statistical analyses were performed with one-way ANOVA with the Turkey post hoc test. * $P < 0.05$, ** $P < 0.01$, *** $P < 0.001$

Pkd1^{delta/delta}.Ezh2^{delta/delta} mice vs. *Pkd1^{delta/delta}.Ezh2^{+/+}* mice (Fig. 6G). H&E result found that *Ezh2* knockout had better cystic effect in cortex than in medulla (Fig. 6H). *Pkd1^{delta/delta}.Ezh2^{+/+}* mice had increased cystic epithelial cell proliferation in the kidneys compared with WT mice (Fig. 6I). Ki67-positive cells were significantly decreased in the kidneys of *Pkd1^{delta/delta}.Ezh2^{delta/delta}* mice. Our previous data showed that STAT3 was over-activated in polycystic kidneys, and inhibition of STAT3 by triptolide reduced cyst growth in a PKD rat model [26]. The protein expression of EZH2, phosphorylation of STAT3 (p-STAT3), and H3K27me3 were increased in kidneys from *Pkd1^{delta/delta}.Ezh2^{+/+}* mice vs. WT mice, whereas the expression of the three proteins decreased in kidneys from *Pkd1^{delta/delta}.Ezh2^{delta/delta}* mice vs. *Pkd1^{delta/delta}.Ezh2^{+/+}* mice (Fig. 6J and K).

EZH2 inhibitor GSK126 suppresses cyst growth in *Pkd1* knockout mice

The effect of GSK126 on ADPKD was first tested in early-onset *Pkd1^{delta/delta}* mice (Fig. 7A). GSK126 (30 mg/kg) reduced the 2KW/BW ratio, BUN, and serum creatinine levels in the *Pkd1^{delta/delta}* mice by 20%, 62%, and 61%, respectively (Fig. 7B). GSK126 significantly delayed cyst growth, as indicated by a 36% decrease in the cyst index compared with age-matched DMSO-treated *Pkd1^{delta/delta}* mice ($P < 0.001$) (Fig. 7C). Moreover, GSK126 significantly inhibited cystic epithelial cell proliferation in the kidneys of *Pkd1^{delta/delta}* mice by Ki-67 staining (Fig. 7D). To mimic the human long-term ADPKD process, we further tested effects of GSK126 on renal cyst growth in late-onset *Pkd1^{delta/delta}* mice with a 5-month follow-up. We administered GSK126 (30 mg/kg) to mice through i.p. injections from P56 to P150. We found that GSK126 treatment delayed cyst growth as indicated by a decreased cyst index, KW/BW ratio, proliferation of cystic epithelial cells, BUN, and serum creatinine levels (Fig. 7E-H). These results suggested that targeting EZH2 with pharmacological inhibition could delay cyst growth during both short-term and long-term periods in vivo.

Total image scanning indicated that cysts were inhibited in both the medulla and cortex in early-onset *Pkd1^{delta/delta}* mice (Fig. 8A). Immunohistochemical analysis indicated that expressions of EZH2, H3K27me3, p-STAT3, and PCNA were significantly decreased after GSK126 treatment in *Pkd1^{delta/delta}* mice (Fig. 8B, C). Meanwhile, western blotting revealed expressions of EZH2, p-STAT3, and H3K27me3 were decreased in GSK126-treated *Pkd1^{delta/delta}* mice kidneys compared with DMSO control group, whereas STAT3 level did not change significantly (Fig. 8D, E).

EZH2 increases cystic epithelial cell proliferation and phosphorylation of STAT3 in ADPKD

Given the evidence that EZH2 promoted renal cyst growth in vivo, we investigated the function and mechanism involved in the process in vitro. EZH2 mRNA level was knocked down by siRNA and over-expressed by EZH2 plasmids in WT9-12 cells (Fig. 9A). MTT assay showed that knockdown of *Ezh2* by siRNA reduced the proliferation of WT9-12 cells while EZH2 plasmids increased the proliferation of WT9-12 cells at 5 days. WT9-12 cells were treated with various GSK126 concentrations (0, 5, and 10 μ M) for 7 days, and the proliferation index was dose-dependent decreased (Fig. 9B). By using EZH2 siRNA, western blotting showed that expressions of EZH2, H3K27me3, and p-STAT3 were decreased in WT9-12 cells, whereas the expression of STAT3 was almost unchanged (Fig. 9C, D). By using EZH2 plasmid, EZH2, p-STAT3, and H3K27me3 were increased in WT9-12 cells, while the expression of STAT3 was almost unchanged (Fig. 9C, D). WT9-12 cells and RCTEC were treated with GSK126 concentrations (0, 5, and 10 μ M) for 5 days, and protein expressions of EZH2, H3K27me3, and p-STAT3 were dose-dependent decreased (Fig. 9E, F). Considering the time effect, WT9-12 cells were treated with 10 μ M GSK126 concentrations for 2 days. EZH2, p-STAT3, and H3K27me3 protein levels were remarkably inhibited at 24 H and 48 H, while STAT3 was almost unchanged (Fig. 9G, H).

EZH2 activates STAT3 by methylation in ADPKD

To further investigate the mechanisms mediated by EZH2, EZH2 was pulled down from WT9-12 cell protein samples with antibodies by IP to detect its binding proteins. We determined that endogenous EZH2 could precipitate with STAT3 by immunoprecipitation in WT9-12 cell proteins (Fig. 9I). To investigate whether the interaction between EZH2 and STAT3 affected their methylation, STAT3 was pulled down from cell protein samples with an anti-methylation antibody. We found that the methylation of STAT3 was positive in WT9-12 cells, and the inhibition of EZH2 with GSK126 dose-dependently decreased the methylation of STAT3 (Fig. 9J). In addition, EZH2 was pulled down from human ADPKD kidneys by IP to detect its binding proteins. We showed that STAT3 was also enriched with EZH2 antibodies in the immunoprecipitates (Fig. 9K). Then, we pulled down STAT3 in kidneys from normal human controls and ADPKD patients and found that STAT3 methylation was more enhanced in ADPKD tissues than in normal controls (Fig. 9L). These results together with those for knockdown of *Ezh2* or inhibition with GSK126 leading to a decreased phosphorylation of STAT3, suggested that EZH2 might regulate STAT3 activation in *Pkd1* mutant tissues and cells through methylation of the substrates.

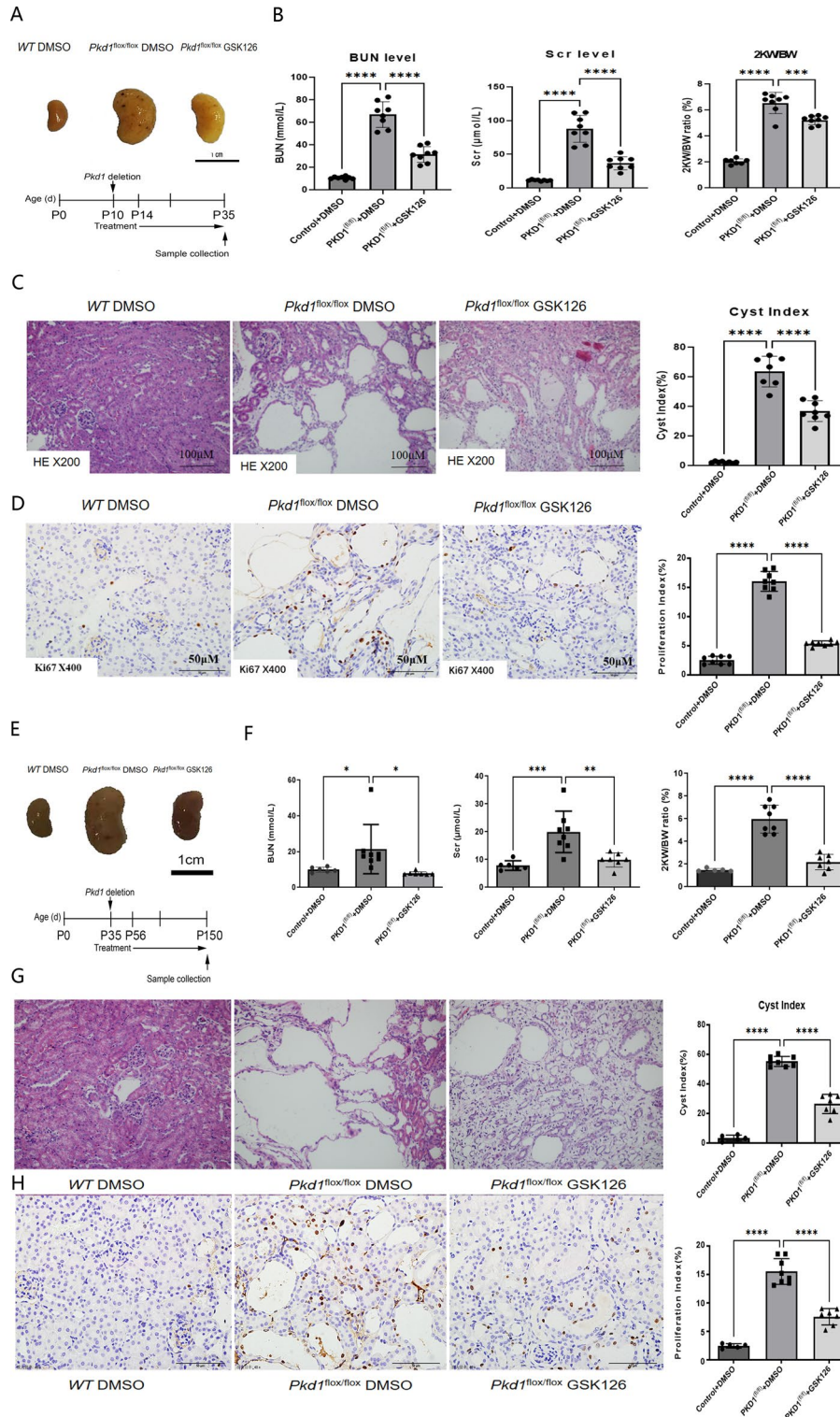


Fig. 7 GSK126 treatment suppresses cyst growth in both early-onset and late-onset *Pkd1*^{delta/delta} mice. **(A)** Representative kidneys from *Pkd1*^{+/+} DMSO control (n=8), *Pkd1*^{delta/delta} (*Pkd1*^{flox/flox}) DMSO control (n=8), and *Pkd1*^{delta/delta} GSK126 mice (n=8) from P14 to P35. Scale bar: 1 cm. Schedule of the treatment of *Pkd1* conditional knockout mice (bottom panel). **(B)** Treatment with GSK126 compared with DMSO decreased serum BUN, creatinine levels, and 2KW/TBW ratios in *Pkd1*^{+/+} mice. **(C)** The cyst index in P35 kidneys. **(D)** The percentage of Ki67-positive nuclei in cells was calculated from a mean of 1,000 nuclei per kidney section. Scale bar: 50 μm. **(E)** Representative kidneys from *Pkd1*^{+/+} DMSO control (n=6), *Pkd1*^{delta/delta} DMSO control (n=8), and *Pkd1*^{delta/delta} GSK126 mice (n=7) from P56 to P150. Scale bar: 100 μm. **(F)** Treatment with GSK126 compared with DMSO decreased serum BUN, creatinine levels, and 2KW/TBW ratios in late-onset *Pkd1*^{delta/delta} mice. **(G)** The cyst index in P150. **(H)** Ki67 staining in P150. Scale bar: 50 μm. Statistical analyses were performed with one-way ANOVA with the Turkey post hoc test. **P* < 0.05, ***P* < 0.01, ****P* < 0.001

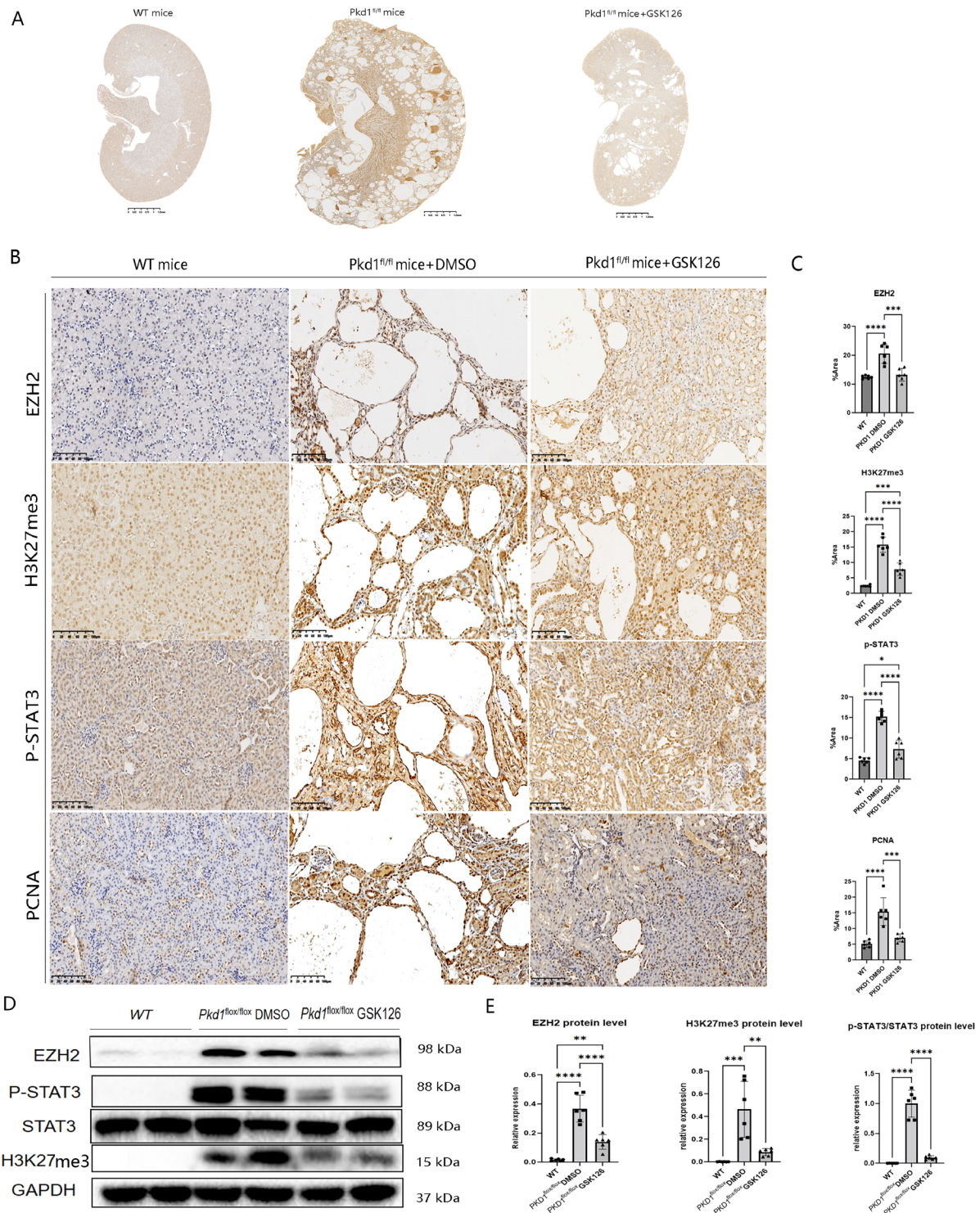


Fig. 8 GSK126 treatment inhibits p-STAT3 and PCNA in *Pkd1^{delta/delta}* mice kidneys. **(A)** Total image scanning of histological kidneys on P25 from *Pkd1^{+/+}* DMSO control, *Pkd1^{delta/delta}* (*Pkd1^{lox/lox}*) DMSO control, and *Pkd1^{delta/delta}* GSK126 mice. **(B and C)** Immunohistochemical analysis indicated that EZH2, H3K27me3, p-STAT3, and PCNA expression were decreased in GSK126-treated *Pkd1^{delta/delta}* mice kidneys compared with *Pkd1^{delta/delta}* mice kidneys, $N=6$ respectively. **(D)** Western blotting of EZH2, p-STAT3, STAT3, and H3K27me3 expression from WT DMSO control, *Pkd1^{delta/delta}* DMSO control, and *Pkd1^{delta/delta}* GSK126 mice at P35, $N=6$ respectively. **(E)** The expression of EZH2, p-STAT3/STAT3, and H3K27me3 were decreased in kidneys from *Pkd1^{delta/delta}* GSK126 mice compared with DMSO control group, whereas STAT3 did not change significantly. Statistical analyses were performed with one-way ANOVA with the Turkey post hoc test. ** $P < 0.01$, *** $P < 0.001$, **** $P < 0.0001$

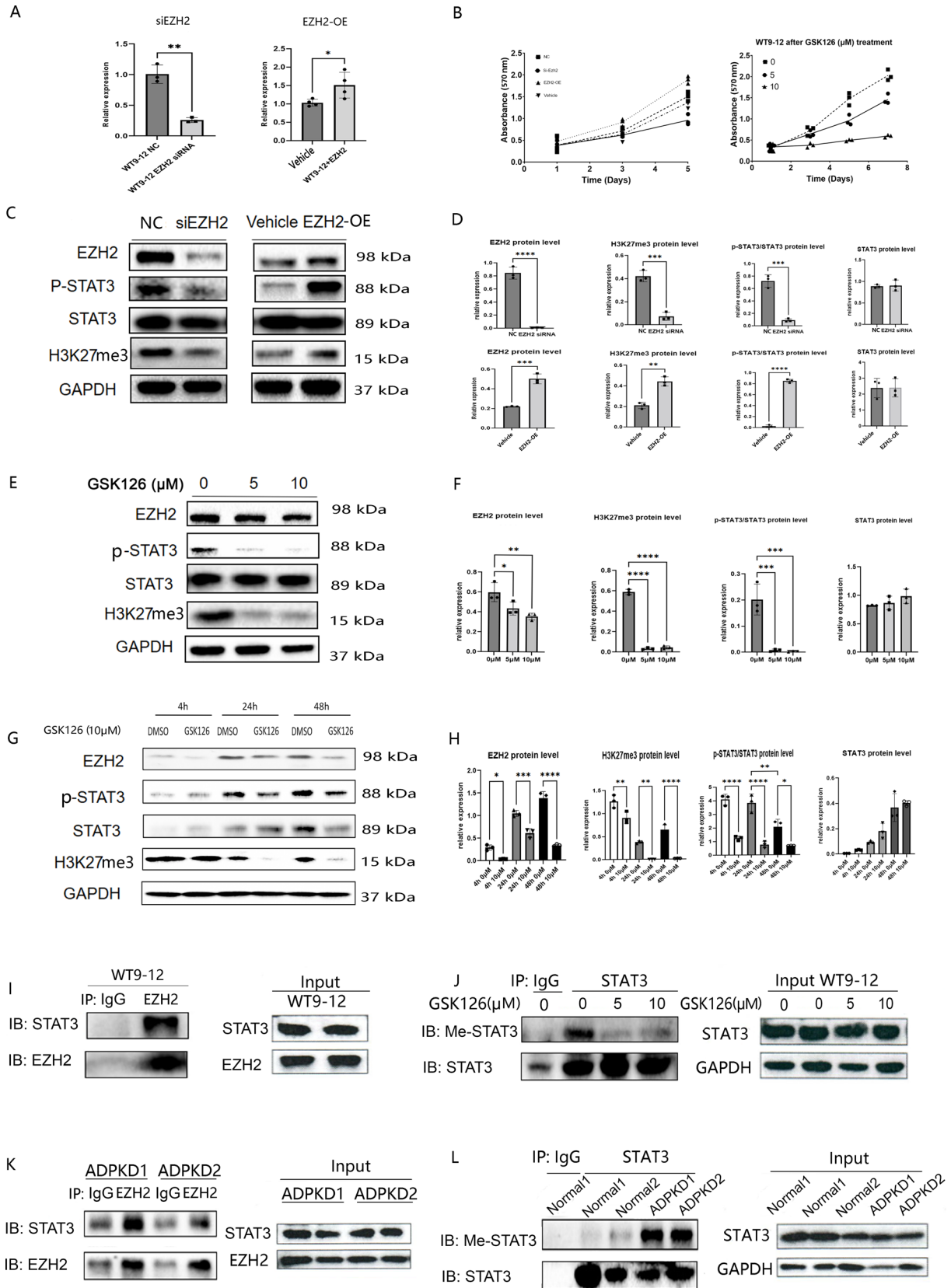


Fig. 9 (See legend on next page.)

(See figure on previous page.)

Fig. 9 EZH2 increases WT9-12 cell proliferation and activates STAT3 by methylation. **(A)** EZH2 mRNA level was knocked down by siRNA and over-expressed by EZH2 plasmids in WT9-12 cells. WT9-12 NC group consisted of WT9-12 cells transfected with a non-coding siRNA, which served as the control for EZH2 siRNA group. The vehicle group consisted of WT9-12 cells transfected with the empty plasmid, serving as the control for the EZH2 overexpression (EZH2-OE) experiments. **(B)** The MTT assay showed that knockdown of *Ezh2* by siRNA reduced the proliferation of WT9-12 cells while EZH2 plasmids increased the proliferation of WT9-12 cells at 5 days. WT9-12 cells were treated with various GSK126 concentrations (0, 5, and 10 μ M) for 7 days. **(C and D)** By using EZH2 siRNA, western blotting expressions of EZH2, H3K27me3, and p-STAT3 were decreased in WT9-12 cells, whereas the expression of STAT3 was almost unchanged. By using EZH2 plasmid, EZH2, p-STAT3, and H3K27me3 were increased in WT9-12 cells, while the expression of STAT3 was almost unchanged. **(E and F)** WT9-12 cells and RCTEC were treated with GSK126 concentrations (0, 5, and 10 μ M) for 5 days, western blotting expressions of EZH2, H3K27me3, and p-STAT3 were dose-dependent decreased. **(G and H)** WT9-12 cells were treated with 10 μ M GSK126 concentrations for 2 days. EZH2, p-STAT3, and H3K27me3 protein levels were remarkably inhibited while expressions of STAT3 were almost unchanged. **(I)** Interactions between EZH2 and STAT3 in WT9-12 cells were detected with anti-EZH2 antibody and then blotted with anti-STAT3 antibody. IgG was the negative control. **(J)** WT9-12 cells were immunoprecipitated with anti-STAT3 antibody and then blotted with anti-methylated lysine antibody. The methylated STAT3 level was decreased in WT9-12 cells treated with GSK126 (5 and 10 μ M, 3 days) compared with WT9-12 cells treated with DMSO. **(K)** Interactions between EZH2 and STAT3 in human ADPKD kidney tissues (1 and 2) were also detected with an anti-EZH2 antibody and blotted with an anti-STAT3 antibody. **(L)** Methylation of STAT3 was increased in two different human ADPKD kidney tissues compared with two normal controls. Kidney tissues were immunoprecipitated with anti-STAT3 antibody and then blotted with anti-methylated lysine antibody. IgG was the negative control. Statistical analyses were performed with an unpaired t-test or one-way ANOVA with the Turkey post hoc test. * $P < 0.05$, ** $P < 0.01$, *** $P < 0.001$, **** $P < 0.0001$

Predicted structure and binding interaction between EZH2 and STAT3 protein was modeled by AlphaFold in Supplement 4. Moreover, STAT3 mediates the activation of c-Myc gene by binding to specific regions in c-Myc promoter [27].

EZH2 promotes cell cycle and activates wnt signaling in human cyst epithelial cells

To identify the EZH2-regulated genes responsible for cystogenesis, RNA sequencing was performed from WT9-12 and WT9-12+EZH2 siRNA cell groups. We found 809 upregulated and 826 downregulated DEGs (Fig. 10A, B). KEGG analysis found that DEGs were abundant in metabolic pathways, cell cycle, Wnt signaling pathways, ferroptosis, etc. Thus, the expression of P21 and β -catenin were further evaluated. By specific knockdown of EZH2 by siRNA, protein levels of non-p- β -catenin, EZH2, and H3K27me3 were decreased in WT9-12 cells compared with RCTEC, whereas the expression of p21 was over-expressed (Fig. 10C, D). β -catenin was almost unchanged. WT9-12 cells and RCTEC then were treated with GSK126 concentrations (0, 5, 10, and 20 μ M) for 2 days, western blotting showed that expressions of EZH2, H3K27me3, and non-p- β -catenin were dose-responsively decreased from 5 to 20 μ M, whereas GSK126 dose-responsively increased the expression of p21 (Fig. 10E, F). β -catenin was almost unchanged. We repeated the experiments in OX161 and Ucl93 cells, and the results were stable (Supplement 6). Predicted structure and binding interaction between EZH2 and non-p- β -catenin protein was modeled by AlphaFold in Supplement 7. Cell cycle analysis at 2 days confirmed that there was a significant reduction in the percentage of cells in the S and G2 phases accompanied by an increase in the percentage of cells in the G0/G1 phase after GSK126 treatment in WT9-12 and OX161 cells (Fig. 10G, H). GSK126 dose-responsively increased the percentage of G0/G1 cells from 5 to 20 μ M. Besides, we found that mRNA levels

of TNF- α upregulated in WT9-12 cells compared with RCTEC (Supplement 8). Knockdown of *Ezh2* and inhibition with GSK126 decreased TNF- α mRNA level.

EZH2 enhances ferroptosis by inhibiting SLC7A11 and GPX4 in ADPKD

As ferroptosis was a key pathway indicated by EZH2-regulated DEGs responsible for cell cystogenesis, we hypothesized that EZH2 might promote ferroptosis in ADPKD. Initially, RT-PCR results indicated reduced mRNA levels of glutathione peroxidase 4 (GPX4, a key ferroptosis inhibitor) and SLC7A11 (a glutamate/cystine antiporter essential for glutathione synthesis) in human ADPKD kidney tissues compared to normal controls. However, the mRNA levels of Acyl-CoA Synthetase Long-Chain Family Member 4 (ACSL4, a ferroptosis promoter via lipid peroxidation) showed no significant difference (Fig. 11A). mRNA levels of GPX4, SLC7A11 were also lower, while ACSL4 was higher in *Pkd1*^{-/-} cells vs. *Pkd1*^{+/-} cells (Fig. 11B). Western blotting revealed that GPX4 and SLC7A11 protein expressions were significantly decreased, and ACSL4 was slightly increased in *Pkd1*^{delta/delta} mice kidneys compared to WT mice (Fig. 11C). Quantifications of Western blotting were shown in Supplement 9.

Moreover, knockdown of *Ezh2* by siRNA increased mRNA and protein levels of GPX4 and SLC7A11 in *Pkd1*^{-/-} cells vs. *Pkd1*^{+/-} cells with minimal effect on ACSL4 levels (Fig. 11B, E). Western blotting showed that GSK126-mediated inhibition of EZH2 moderately upregulated GPX4 and SLC7A11 protein levels without affecting ACSL4 protein levels in *Pkd1*^{-/-} cells (Fig. 11D). Prussian blue staining and 4HNE staining revealed increased 4HNE and Fe3+ deposition, while XCT showed decreased SLC7A11 expression in *Pkd1*^{delta/delta} mice kidneys compared with WT mice and *Pkd1*^{delta/delta} + DMSO mice kidneys versus WT mice, respectively (Fig. 11F). In contrast, *Pkd1* and *Ezh2* double conditional

knockout and GSK126 treatment both reduced 4HNE and Fe³⁺ deposition while increasing SLC7A11 expression (Fig. 11G). These findings suggest that EZH2 may enhance ferroptosis by inhibiting SLC7A11 and GPX4 in ADPKD. The schematic model of EZH2 in ADPKD was listed in Fig. 12 and Supplement 10.

Discussion

Epigenetics plays important roles in ADPKD pathogenesis [7, 10, 11]. In this study, we studied the functions of EZH2 in the setting of cyst growth, revealing its upregulation across various ADPKD models and assessing the therapeutic potential of EZH2 inhibition on cystogenesis. Our findings indicated a significant increase in EZH2 mRNA and protein levels in vivo and in vitro. *PKD1/2* mutation may activate cAMP/PKA/CREB pathway and increase EZH2 expression in ADPKD. Importantly, the inhibition of EZH2, through pharmacological means or gene knockdown, markedly attenuated cyst formation and growth, underscoring EZH2's pivotal role in PKD pathogenesis. EZH2-specific inhibitor, GSK126, could delay cyst growth and protect renal function in both early and late-onset *Pkd1* knockout mice. EZH2 mediated cystogenesis by enhancing methylation and activation of STAT3, stimulating non-phosphorylated β -catenin in Wnt signaling pathway, and suppressing p21. Additionally, EZH2 enhanced ferroptosis by inhibiting SLC7A11 and GPX4.

An interesting finding was the different EZH2 expression among kidney cell types in ADPKD. SnRNA-seq data showed that EZH2 had higher expression in the proximal tubule cells, ascending thin limb, thick ascending limb, and collecting duct cells in ADPKD, which was following origins of cysts in various segments of renal tubules [28]. However, EZH2 expression was not significantly increased at distal tubules, which may partly decipher better cyst suppression at cortex after EZH2 knockout in PKD mice. It is noteworthy that GSK126 inhibition suppressed cyst growth in both cortex and medulla, which was not affected by EZH2 knockout efficiency.

The upregulation of EZH2 in PKD observed in our study aligned with previous cancer research [12, 13]. The upregulation of EZH2 in ADPKD and the beneficial effects of its inhibition on cystogenesis, as observed in our study, sit at the confluence of a growing body of literature exploring EZH2's role. EZH2 research has predominantly focused on its oncogenic functions in cancer biology, where EZH2 is known to facilitate tumorigenesis through the epigenetic silencing of genes that regulate cell cycle arrest and apoptosis. In cancer research, EZH2's overexpression has been consistently linked to poor prognosis and aggressive disease phenotypes, prompting the development of EZH2 inhibitors as therapeutic agents [29]. Studies in lymphoma and solid tumors

have shown that targeting EZH2 can halt tumor growth and even reverse the malignant phenotype. ADPKD is a tumor-like disease to some degree [30]. The inhibition of EZH2 in ADPKD models leading to reduced cyst growth partly mirrors the inhibitory effects of EZH2 targeting in cancers. However, our work first elucidated the multifaceted role of EZH2 across human samples and multiple PKD models in ADPKD, from gene expression regulation to its involvement in critical signaling pathways like STAT3, p21, Wnt, and ferroptosis. The efficacy of EZH2 inhibitors (GSK126 and EPZ-6438) in reducing cyst growth in our study contributed significantly to the literature, highlighting EZH2 as a viable therapeutic target for ADPKD.

We hypothesized that polycystin-1/2 regulated EZH2 expression through the cAMP/PKA/CREB pathway. Dysfunction of polycystins could promote cell proliferation by increasing the cellular level of adenosine 3',5'-cyclic monophosphate (cAMP), which in turn activates protein kinase A (PKA) and downstream transcriptional factor CREB [31]. The cellular level of cAMP is elevated in ADPKD, which plays a central role in the progression of ADPKD by stimulating fluid secretion and cell proliferation [32]. We partly proved this hypothesis with the following results: (1) p-CREB positively correlated with EZH2 expression in ADPKD kidneys; (2) cAMP agonists or antagonists increased or decreased CREB phosphorylation and EZH2 expression respectively; (3) inhibition of CREB activity by PKA inhibitor H89 down-regulated EZH2 expression; (4) knockdown CREB by siRNA decreased EZH2 expression, and vice versa CREB overexpression increased EZH2 expression. Our findings suggest that EZH2 upregulation and cyst growth may form a positive feedback loop, where each process amplifies the other. Elevated cAMP levels, commonly observed in cystic cells, were found to enhance EZH2 expression, while increased EZH2 activity further drives cystogenesis. This mutual reinforcement between EZH2 upregulation and cyst growth likely contributes to the progressive nature of the disease, creating a cycle that accelerates cyst development over time.

We found that the methylation level of H3K27 was enhanced in animal and human polycystic kidney tissues and EZH2 inhibition or ablation decreased H3K27me3 in vivo and in vitro, implying that EZH2 may promote renal cyst growth through epigenetically regulating target gene expression. EZH2 is well known for its role in maintaining the repression of multiple downstream targets such as HOX, e-cadherin, FOXC1, and DNA damage repair pathways through epigenetically modifying histones [33, 34]. Additionally, EZH2 directly influences DNA methylation and interacts with DNA methyltransferases within the PRC2/3, indicating a direct connection between two key epigenetic repression systems [35]. Besides, EZH2

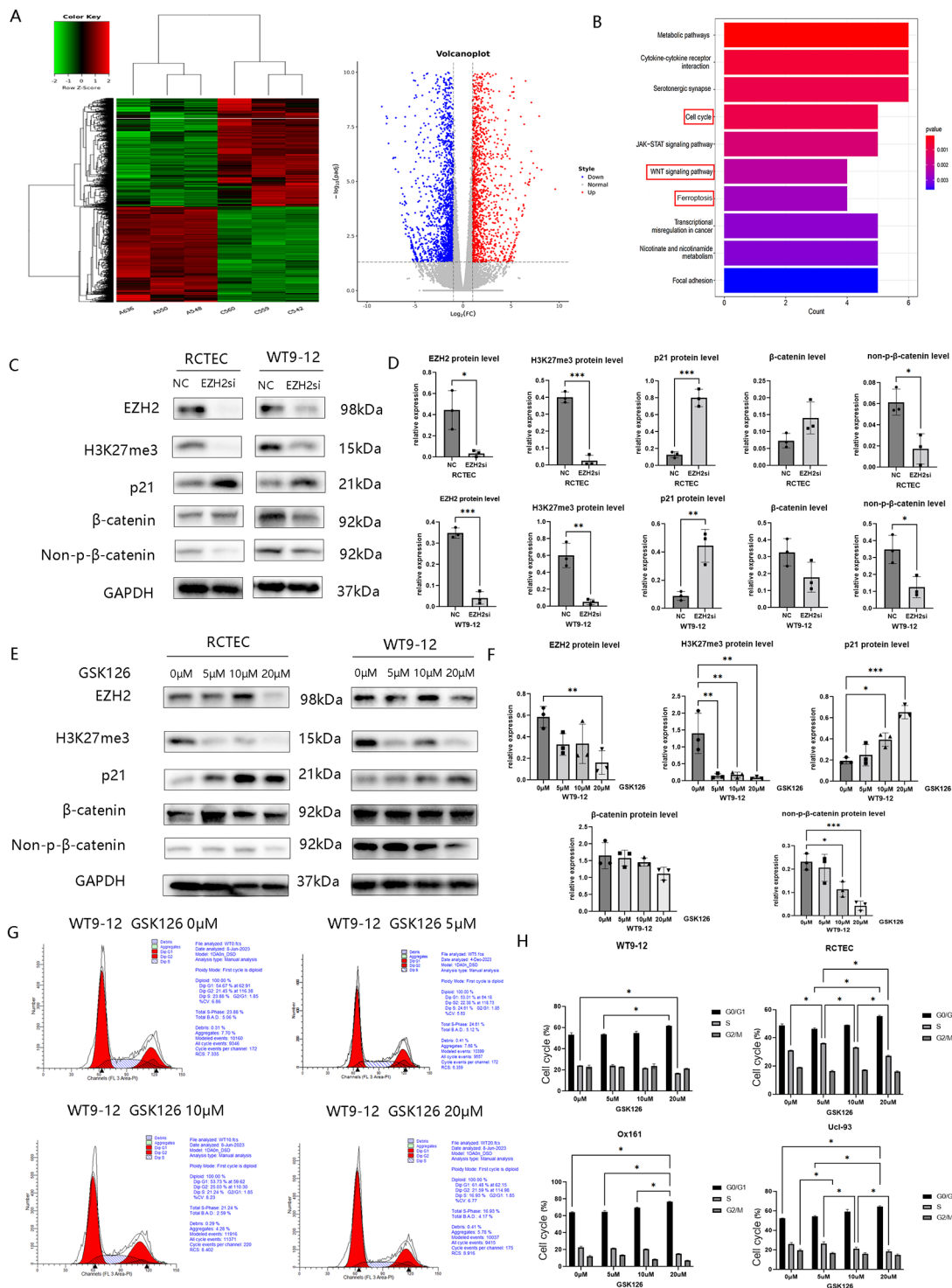


Fig. 10 Inhibition of EZH2 decreases non-p-β-catenin and arrests cell cycle by p21 in vitro. **(A)** Heatmap and volcano map of 809 upregulated and 826 downregulated DEGs from RNA sequencing performed from WT9-12 and WT9-12+EZH2 siRNA cells. **(B)** KEGG enrichment analysis of DEGs. **(C and D)** By using EZH2 siRNA, western blotting expressions of EZH2, H3K27me3, and non-p-β-catenin were decreased in WT9-12 cells vs. RCTEC, whereas the expression of p21 was over-expressed. β-catenin was almost unchanged. **(E and F)** WT9-12 cells and RCTEC were treated with GSK126 concentrations (0, 5, 10, and 20 μM) for 2 days, western blotting expressions of EZH2, H3K27me3, and non-p-β-catenin were dose-dependently decreased, whereas the expression of p21 was over-expressed. β-catenin was almost unchanged. **(G)** Stages of the cell cycle of WT9-12 cells treated with GSK126 concentrations (0, 5, 10, and 20 μM) at 5 days. **(H)** G0/G1 phase, S phase, and G2/M phase percent of cell cycle in WT9-12 cells, RCTEC, OX161, and Ucl93 cells treated with GSK126 concentrations (0, 5, 10, and 20 μM) at 2 days, respectively. Statistical analyses were performed with an unpaired t-test or one-way ANOVA with the Turkey post hoc test. **P*<0.05, ***P*<0.01, ****P*<0.001

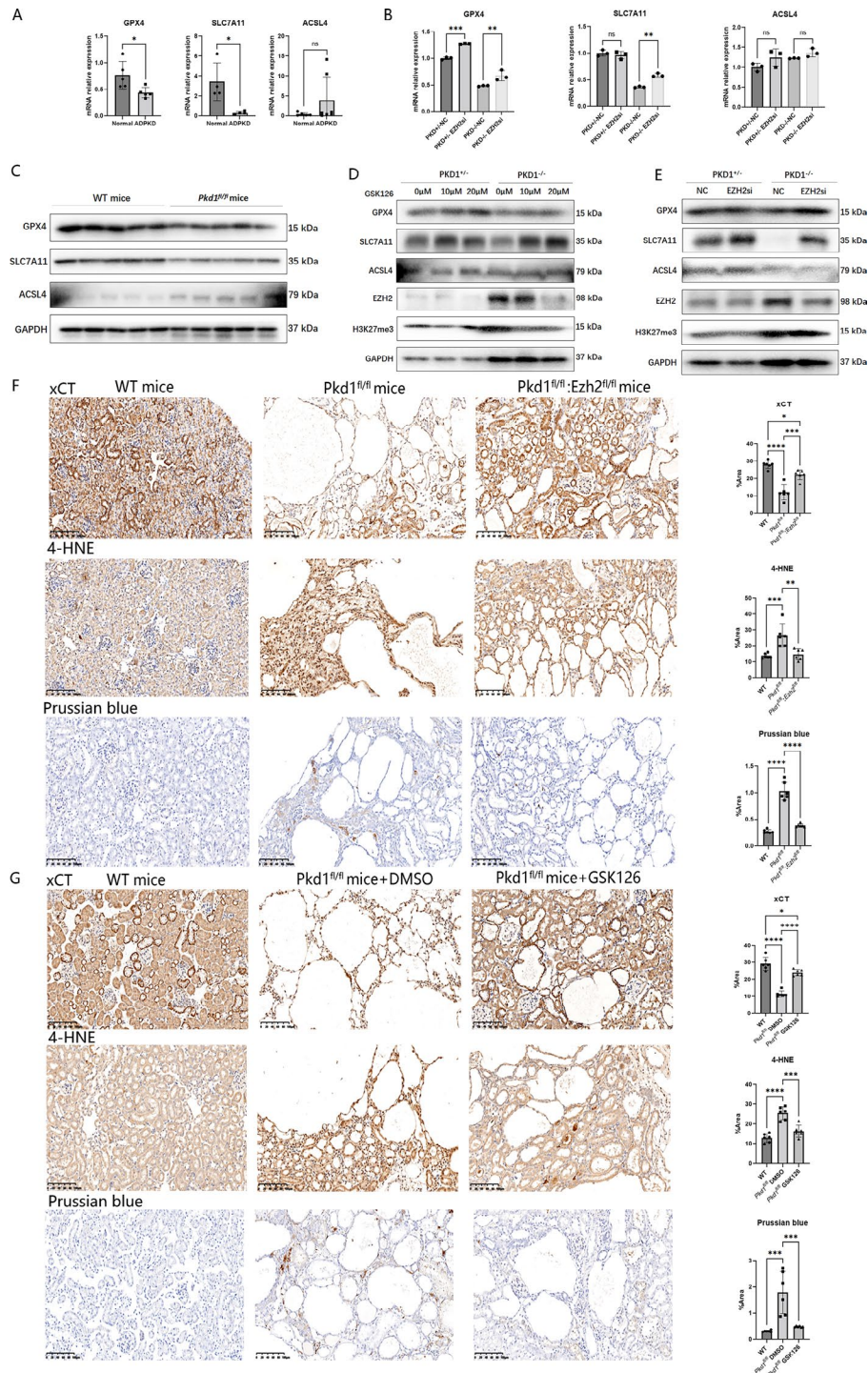


Fig. 11 EZH2 enhances ferroptosis by inhibiting SLC7A11 and GPX4 in ADPKD. **(A)** mRNA expression levels of GPX4, SLC7A11, and ACSL4 in human ADPKD kidney tissues vs. normal controls. **(B)** mRNA levels of GPX4, SLC7A11, and ACSL4 in *Pkd1*^{-/-} cells vs. *Pkd1*^{+/-} cells. The effect of *Ezh2* knockdown on mRNA levels of GPX4, SLC7A11, and ACSL4 in *Pkd1*^{-/-} cells vs. *Pkd1*^{+/-} cells. **(C)** Western blotting of protein expressions of GPX4, SLC7A11, and ACSL4 in *Pkd1*^{delta/delta} (*Pkd1*^{fl/fl}/*fl*) mice kidneys vs. WT mice. **(D)** Western blotting of protein expressions of GPX4, SLC7A11, and ACSL4 after inhibition of EZH2 by different doses of GSK126 in *Pkd1*^{-/-} cells vs. *Pkd1*^{+/-} cells. **(E)** The effect of *Ezh2* knockdown on protein levels of GPX4, SLC7A11, and ACSL4 in *Pkd1*^{-/-} cells vs. *Pkd1*^{+/-} cells. **(F)** xCT, 4HNE, and Prussian blue staining analysis in *Pkd1*^{+/-};Ezh2^{+/+} mice, *Pkd1*^{delta/delta};Ezh2^{+/+} mice, and *Pkd1*^{delta/delta};Ezh2^{delta/delta} (*Pkd1*^{fl/fl}/*fl*;Ezh2^{fl/fl}/*fl*) mice kidneys. **(G)** xCT, 4HNE, and Prussian blue staining analysis in *Pkd1*^{+/-} DMSO control, *Pkd1*^{delta/delta} DMSO control, and *Pkd1*^{delta/delta};GSK126 mice. Statistical analyses were performed with an unpaired t-test or one-way ANOVA with the Turkey post hoc test. **P* < 0.05, ***P* < 0.01, ****P* < 0.001

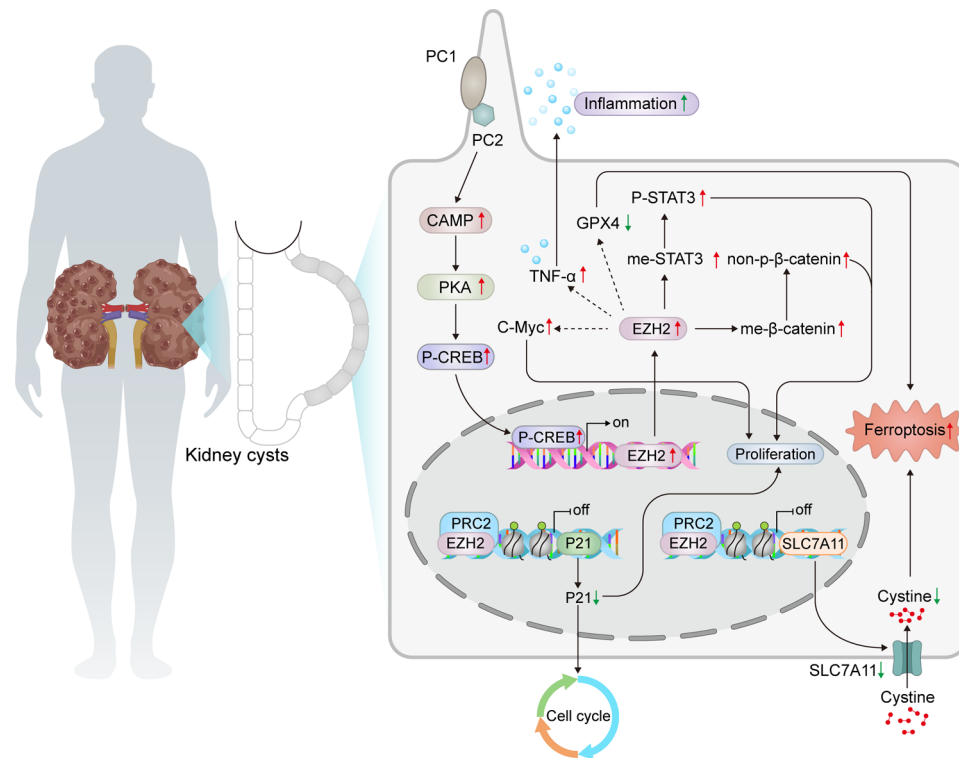


Fig. 12 A schematic model for the mechanism of EZH2 in cyst growth of ADPKD. *Pkd1/2* mutation or knockout results in the upregulation of cAMP/PKA/CREB signaling. Upregulated EZH2 methylated STAT3 leading to its phosphorylation and increased proliferation by activating STAT3 and Wnt signaling pathways, promoted cell cycle by inhibiting p21 signaling, increased ferroptosis by inhibiting GPX4 and SLC7A11, and regulated the transcription of potential targeted genes such as TNF α and c-Myc. Targeting EZH2 with specific inhibitors GSK126 or EPZ-6438 could delay cyst growth in ADPKD

can reduce non-coding RNA expression by binding to the promoter [36]. In addition to its known roles in transcriptional regulation and histone modification, EZH2 can methylate nonhistone substrates [13, 37, 38]. Several studies identified a PRC2-independent role of EZH2 in transcriptional activation instead of repression [39]. For example, an activating function of EZH2 was found in breast cancer via activation of NF- κ B targets [40]. EZH2 has been shown to methylate the androgen receptor and modulate its recruitment in a prostate cancer model [40]. In this study, we found that STAT3 was a nonhistone substrate of EZH2. We found that the upregulation of EZH2 led to the methylation and phosphorylation of STAT3 which accelerated cyst proliferation. These data suggested that EZH2 ablation in ADPKD inhibited cell proliferation partly through post-translational modification of STAT3. Moreover, co-IP results indicate that EZH2 is directly bound with me-STAT3 in ADPKD. Dasgupta et al. [37] found that K49 of STAT3 was dimethylated by EZH2 and that EZH2 preferentially bound to tyrosine-phosphorylated STAT3. The amino acid sequence surrounding the K49 methylation site of STAT3 and the H3K27 EZH2-dependent methylation site were similar, which may lead to binding between EZH2 and STAT3 in ADPKD. [37] Moreover, C-Myc, a downstream regulatory gene of

STAT3, was inhibited by knockdown of *Ezh2* or GSK126 treatment in vitro. C-Myc is a well-known oncogene that regulates cell cycle progression, apoptosis, and cellular transformation [2]. Therefore, EZH2 might increase cyst growth by activating me-STAT3/c-Myc signaling.

Our study indicated that the modulation of EZH2, either through siRNA knockdown or pharmacological inhibition using GSK126, impacted p21 expression. Notably, the downregulation of EZH2 led to decreased levels of H3K27me₃, alongside an overexpression of p21 in WT9-12 cells when compared to RCTEC. Furthermore, the increase in p21 expression following *Ezh2* knockdown or GSK126 treatment indicated a possible mechanism by which EZH2 influenced cell cycle arrest in the G₀/G₁ phase, thereby reducing the progression of cells into the S and G₂ phases. The mechanism by which EZH2 regulated p21 involved the trimethylation of H3K27me₃, leading to the repression of p21 expression [41]. Besides, EZH2 can influence the expression of p21 indirectly through its role in chromatin remodeling and gene silencing [42]. In melanoma cells, EZH2 suppression led to the activation of p21/CDKN1A in a p53-independent manner, contributing significantly to cell cycle arrest and the induction of a senescence phenotype [42].

Moreover, *Ezh2* knockdown or using GSK126 inhibited Wnt signaling in vitro. The downregulation of EZH2 dose-dependently led to decreased levels of non-phosphorylated β -catenin. This suggested that EZH2 inhibition decreased β -catenin's activity, which is a key component of the Wnt signaling known for its role in controlling cell proliferation and differentiation in ADPKD [43]. EZH2 regulated non-phosphorylated β -catenin in colorectal cancer through a specific mechanism involving the activation of the AKT pathway [44]. When AKT is activated, it phosphorylates EZH2 on serine 21. This phosphorylation event is crucial for enabling EZH2 to interact with and methylate β -catenin at lysine 49 (K49) [44]. This methylation of β -catenin increased its binding affinity to chromatin. EZH2- β -catenin interactions are associated with colorectal cancer progression, including enhancements in cell stemness and migration [44]. Therefore, EZH2 could methylate and activate Wnt/ β -catenin signaling, ultimately increasing cyst growth and progression in ADPKD. Moreover, we found that TNF- α levels were upregulated in WT9-12 cells compared with RCTEC, and that knockdown of *Ezh2* or inhibition with GSK126 significantly decreased TNF- α mRNA levels, highlighting a potential role of EZH2 in activating TNF signaling in ADPKD.

Last, the intriguing link between EZH2 regulation and ferroptosis added a novel layer to the understanding of ADPKD pathogenesis. Ferroptosis, a form of regulated cell death driven by iron-dependent lipid peroxidation, emerged as a pivotal pathway influenced by EZH2-regulated DEGs involved in cystogenesis. EZH2 disrupted the cellular antioxidant defense and enhanced susceptibility to ferroptotic cell death, contributing to the progression of renal cystogenesis [45]. Our results revealed that EZH2 may promote ferroptosis by downregulating key inhibitors such as glutathione GPX4 and the glutamate/cystine antiporter SLC7A11. The regulatory mechanism involved EZH2 suppressing SLC7A11 expression through H3K27me3 modification [46]. The observed upregulation of SLC7A11 upon EZH2 inhibition suggested that EZH2 suppression of SLC7A11 fostered a ferroptotic environment conducive to ADPKD progression. However, the regulation of GPX4 by EZH2 is not yet fully understood. It is possible that EZH2 directly binds to the promoter regions of GPX4, promoting H3K27me3 modification and resulting in the silencing of GPX4 expression, or it may interact with microRNAs and transcription factors that further modulate GPX4 expression. Collectively, these findings highlight the role of EZH2 in regulating ferroptosis through mechanisms involving the repression of GPX4 and SLC7A11. Understanding these pathways enhances our appreciation of the potential of EZH2 inhibitors as therapeutic agents in ADPKD by mitigating ferroptosis.

EZH2 has become an important therapeutic target for cancer therapy [47]. Our study proved that EZH2 regulated several physiological processes in cyst development and enlargement, highlighting the potential therapeutic relevance of targeting EZH2 in ADPKD. The small molecule EZH2 inhibitor, GSK126, inhibited both mutant and wild-type EZH2 with an over 1,000-fold selectivity for EZH2 over other methyltransferases [48]. Our study not only showed high expression of EZH2 in human ADPKD but also tested the effect of GSK126 in ADPKD animal models and organoids for the first time and found it could attenuate cyst growth. Moreover, GSK126 decreased EZH2 and H3K27me3 in PKD mice without affecting the survival time. The potential of EZH2 inhibition as a therapeutic strategy opens up new possibilities for PKD treatment, emphasizing the need for further research in this area. These findings are particularly promising considering the limited effective treatments currently available for ADPKD, offering a potential new avenue for therapy development. The development of EZH2 inhibitors, such as EPZ-6438 (Tazemetostat), has opened new avenues for cancer treatment, particularly for malignancies characterized by EZH2 overexpression or mutation [49]. Future research should focus on exploring the long-term impact of EZH2 inhibition on ADPKD progression, particularly in human clinical trials. Investigating the role of EZH2 at different stages of PKD and identifying potential biomarkers for EZH2 activity could provide valuable insights for targeted therapy development. Moreover, examining combinational therapy approaches, including the use of EZH2 inhibitors alongside other therapeutic agents, could enhance treatment efficacy and minimize resistance.

Our study had some limitations. First, we did not assess fibrosis levels in the EZH2 knockout or GSK126-treated mouse models. Secondly, one limitation of our study is the absence of kidney tissue samples from early-stage *Pkd1^{delta/delta}* mice. As a result, we were unable to assess the expression of EZH2 and H3K27me3 during the precystic stages of disease development. Thirdly, we did not directly examine PC1/PC2 mutations and our evidence for the regulation of EZH2 through the cAMP/PKA/CREB pathway was based on indirect pharmacological interventions. Additionally, while exploring tolvaptan and the mTOR pathway could provide further insights, these aspects were beyond the scope of our current study and will be considered for future research.

In conclusion, our investigation revealed significant upregulation of EZH2 in ADPKD and demonstrated the therapeutic potential of EZH2 inhibition in reducing cystogenesis. Abnormal polycystins may increase EZH2 expression via the cAMP/PKA/CREB pathway. EZH2 plays a critical role in ADPKD progression by activating STAT3 and Wnt signaling, promoting the cell cycle

by inhibiting P21, and enhancing ferroptosis by inhibiting SLC7A11 and GPX4. EZH2 inhibition significantly reduced cyst growth both in vitro and in vivo. Both pharmacological inhibition and genetic ablation of EZH2 suppressed renal cyst growth and protected renal function in vivo. These findings advance our understanding of ADPKD pathogenesis and highlight EZH2 as a promising therapeutic target. Continued research in this direction is essential for developing viable treatment strategies for ADPKD, offering hope for improved patient outcomes.

Supplementary Information

The online version contains supplementary material available at <https://doi.org/10.1186/s12967-024-05785-5>.

Supplementary Material 1

Supplementary Material 2

Acknowledgements

We would like to express our gratitude to Professor G. Germino and T. Watnick at Johns Hopkins University School of Medicine for providing the Pkd1^{fl/fl}: tamoxifen-Cre mice. We also thank Prof. Ying Cao at Shanghai Tongji University for facilitating the zebrafish (TAB, Tubigen) rearing according to standard protocols in their laboratory. Additionally, we appreciate Prof. Stefan Somlo from Yale University for supplying the Pkd1^{-/-} (PN24) and Pkd1^{+/-} (PH2) cells. The present work was supported by the following grants: (1) The National Key Research and Development Program of China (2016YFC0901502); (2) The National Natural Science Foundation of China (82200786, 81873595 and 81670612); (3) Shanghai Top Priority Key Clinical Disciplines Construction Project (2017ZZ02009); and (4) Scientific Research Project of Shanghai Municipal Health Bureau (201740193); (5) The National Natural Science Foundation of China (81770658 and 31571337); (6) Tianjin Municipal Science and Technology Commission (15JCYBJC54000). The grant 2–5 to C.M., 6–7 to Y.C. The funders had no role in the study design, data collection, data analysis, interpretation, or writing of the paper. The corresponding author had full access to all the data in the study and had final responsibility for the decision to the submission.

Author contributions

C.X., C.M., and Y.C. designed the study; J.L., B.L., L.F., C.H., X.W., W.Z., C.Z., carried out experiments; J.L. and C.X. analyzed the data; C.X. and J.L. made the figures; Y.C., C.X., Z.M., and C.M. drafted and revised the paper; all authors approved the final version of the manuscript.

Funding

This work was supported by grants from the National Natural Science Foundation of China (82200786, 82070705, 81770670, and 81873595). This work was supported by the Oriental Talent Plan Outstanding Program 2023, Shanghai Municipal Key Clinical Specialty (shslczdzk02503), Shanghai Science and Technology Talent Program (19YF1450300), and Research Projects of Shanghai Science and Technology Committee (17411972100). Shanghai Shenkang Research Physician innovation and transformation ability training program SHDC2022CRD024. Scientific and technological innovation action plan of Shanghai medical innovation research 22Y11905500 special project.

Data availability

The datasets generated during and/or analyzed during the current study are available in supplements or from the corresponding author Cheng Xue upon request (chengxia1568@126.com).

Declarations

Ethics approval and consent to participate

All animal procedures were conducted according to the guidelines of and approved by the Animal Research Committee of the Naval Medical University.

Informed consent was obtained from all subjects. The study was approved by the ethics review board of Changzheng Hospital (CZ2018-0619). The study abided by the Declaration of Helsinki principles.

Conflict of interest

The authors declare no conflict of interest.

Author details

¹Kidney Institute, Division of Nephrology, Shanghai Changzheng Hospital, Second Military Medical University (Naval Medical University), 415 Fengyang Road, Shanghai 200003, China

²Center for Clinical Laboratories, Affiliated Hospital of Guizhou Medical University, Guiyang City, Guizhou Province, China

³Department of Biochemistry and Molecular Biology, 2011 Collaborative Innovation Center of Tianjin for Medical Epigenetics, Tianjin Key Laboratory of Medical Epigenetics, School of Basic Medical Sciences, Tianjin Medical University, 22 Qixiangtai Road, Tianjin 300070, China

⁴Department of Nephrology, Shanghai General Hospital, Shanghai Jiaotong University School of Medicine, Shanghai 200080, China

⁵Institute of Infectious Diseases, Beijing Key Laboratory of Emerging Infectious Diseases, Beijing Ditan Hospital, Capital Medical University, Beijing 100015, China

⁶Beijing Institute of Infectious Diseases, Beijing 100015, China

⁷Outpatient Department, Yangpu Third Military Retreat, Shanghai, China

Received: 7 August 2024 / Accepted: 18 October 2024

Published online: 29 October 2024

References

1. Wuthrich RP, Mei C. Pharmacological management of polycystic kidney disease. *Expert Opin Pharmacother*. 2014;15(8):1085–95.
2. Yang M, Lv J, Gong C, Xue C, Fu L, Chen S, Mei C. Inflammation is more sensitive than cell proliferation in response to Rapamycin treatment in polycystic kidney disease. *Kidney Blood Press Res*. 2024;49(1):60–8.
3. Kotsis F, Boehlke C, Kuehn EW. The ciliary flow sensor and polycystic kidney disease. *Nephrol dialysis Transplantation: Official Publication Eur Dialysis Transpl Association - Eur Ren Association*. 2013;28(3):518–26.
4. Paul BM, Vanden Heuvel GB. *Kidney: polycystic kidney disease*. Wiley Interdisciplinary Reviews Dev Biology. 2014;3(6):465–87.
5. Wallace DP. Cyclic AMP-mediated cyst expansion. *Biochim Biophys Acta*. 2011;1812(10):1291–300.
6. Liu N, Zhuang S. Treatment of chronic kidney diseases with histone deacetylase inhibitors. *Front Physiol*. 2015;6:121.
7. Li X. Epigenetics and autosomal dominant polycystic kidney disease. *Biochim Biophys Acta*. 2011;1812(10):1213–8.
8. Xu J, Xue C, Wang X, Zhang L, Mei C, Mao Z. Chromatin Methylation Abnormalities in autosomal Dominant polycystic kidney disease. *Front Med*. 2022;9:921631.
9. Zhou X, Fan LX, Sweeney WE Jr, Denu JM, Avner ED, Li X. Sirtuin 1 inhibition delays cyst formation in autosomal-dominant polycystic kidney disease. *J Clin Invest*. 2013;123(7):3084–98.
10. Zhou X, Fan LX, Peters DJ, Trudel M, Bradner JE, Li X. Therapeutic targeting of BET bromodomain protein, Brd4, delays cyst growth in ADPKD. *Hum Mol Genet*. 2015;24(14):3982–93.
11. Li LX, Fan LX, Zhou JX, Grantham JJ, Calvet JP, Sage J, Li X. Lysine methyltransferase SMYD2 promotes cyst growth in autosomal dominant polycystic kidney disease. *J Clin Investig*. 2017;127(7):2751–64.
12. Verma SK. Inhibition of the histone lysine methyltransferase EZH2 for the treatment of cancer. *Curr Top Med Chem*. 2015;15(8):714–9.
13. Kondo Y. Targeting histone methyltransferase EZH2 as cancer treatment. *J Biochem*. 2014;156(5):249–57.
14. Liu KL, Zhu K, Zhang H. An overview of the development of EED inhibitors to disable the PRC2 function. *RSC Med Chem*. 2022;13(1):39–53.
15. Su Z, Wang X, Gao X, Liu Y, Pan C, Hu H, Beyer RP, Shi M, Zhou J, Zhang J, et al. Excessive activation of the alternative complement pathway in autosomal dominant polycystic kidney disease. *J Intern Med*. 2014;276(5):470–85.
16. Yin J, Leavenworth JW, Li Y, Luo Q, Xie H, Liu X, Huang S, Yan H, Fu Z, Zhang LY, et al. Ezh2 regulates differentiation and function of natural killer cells through histone methyltransferase activity. *Proc Natl Acad Sci USA*. 2015;112(52):15988–93.

17. Yang Y, Chen M, Zhou J, Lv J, Song S, Fu L, Chen J, Yang M, Mei C. Interactions between macrophages and Cyst-lining epithelial cells promote kidney cyst growth in Pkd1-Deficient mice. *J Am Soc Nephrol*. 2018;29(9):2310–25.
18. Wu M, Wahl PR, Le Hir M, Wackerle-Men Y, Wuthrich RP, Serra AL. Everolimus retards cyst growth and preserves kidney function in a rodent model for polycystic kidney disease. *Kidney Blood Press Res*. 2007;30(4):253–9.
19. Cao Y, Semanchik N, Lee SH, Somlo S, Barbano PE, Coifman R, Sun Z. Chemical modifier screen identifies HDAC inhibitors as suppressors of PKD models. *Proc Natl Acad Sci U S A*. 2009;106(51):21819–24.
20. Woo YM, Bae JB, Oh YH, Lee YG, Lee MJ, Park EY, Choi JK, Lee S, Shin Y, Lyu J, et al. Genome-wide methylation profiling of ADPKD identified epigenetically regulated genes associated with renal cyst development. *Hum Genet*. 2014;133(3):281–97.
21. Shibazaki S, Yu Z, Nishio S, Tian X, Thomson RB, Mitobe M, Louvi A, Velazquez H, Ishibe S, Cantley LG, et al. Cyst formation and activation of the extracellular regulated kinase pathway after kidney specific inactivation of Pkd1. *Hum Mol Genet*. 2008;17(11):1505–16.
22. Yao G, Su X, Nguyen V, Roberts K, Li X, Takakura A, Plomann M, Zhou J. Polycystin-1 regulates actin cytoskeleton organization and directional cell migration through a novel PC1-Pacsin 2-N-Wasp complex. *Hum Mol Genet*. 2014;23(10):2769–79.
23. Wu H, Malone AF, Donnelly EL, Kirita Y, Uchimura K, Ramakrishnan SM, Gaut JP, Humphreys BD. Single-cell transcriptomics of a human kidney allograft Biopsy Specimen defines a diverse inflammatory response. *J Am Soc Nephrol*. 2018;29(8):2069–80.
24. Muto Y, Dixon EE, Yoshimura Y, Wu H, Omachi K, Ledru N, Wilson PC, King AJ, Eric Olson N, Grantham MG, et al. Defining cellular complexity in human autosomal dominant polycystic kidney disease by multimodal single cell analysis. *Nat Commun*. 2022;13(1):6497.
25. Magenheimer BS, St John PL, Isom KS, Abrahamson DR, De Lisle RC, Wallace DP, Maser RL, Grantham JJ, Calvet JP. Early embryonic renal tubules of wild-type and polycystic kidney disease kidneys respond to cAMP stimulation with cystic fibrosis transmembrane conductance regulator(Na+),K(+),2Cl(-) co-transporter-dependent cystic dilation. *J Am Soc Nephrol*. 2006;17(12):3424–37.
26. Jing Y, Wu M, Zhang D, Chen D, Yang M, Mei S, He L, Gu J, Qi N, Fu L, et al. Triptolide delays disease progression in an adult rat model of polycystic kidney disease through the JAK2-STAT3 pathway. *Am J Physiol Ren Physiol*. 2018;315(3):F479–86.
27. Vouquier S, Cheung SH, Li L, Hodgson G, Shaw PE. Anomalous behaviour of the STAT3 binding site in the human c-myc P2 promoter. *Biochem Biophys Res Commun*. 2007;364(3):627–32.
28. Harris PC, Torres VE. Polycystic kidney disease. *Annu Rev Med*. 2009;60:321–37.
29. Bracken AP, Pasini D, Capra M, Prosperini E, Colli E, Helin K. EZH2 is downstream of the pRB-E2F pathway, essential for proliferation and amplified in cancer. *EMBO J*. 2003;22(20):5323–35.
30. Ke Sun DX. The association between autosomal dominant polycystic kidney disease and cancer. *Int Urol Nephrol*. 2019;51:93–100.
31. Aguiari G, Bizzarri F, Bonon A, Mangolini A, Magri E, Pedriali M, Querzoli P, Somlo S, Harris PC, Catzone L, et al. Polycystin-1 regulates amphiregulin expression through CREB and AP1 signalling: implications in ADPKD cell proliferation. *J Mol Med*. 2012;90(11):1267–82.
32. Belibi FA, Reif G, Wallace DP, Yamaguchi T, Olsen L, Li H, Helmkamp GM Jr, Grantham JJ. Cyclic AMP promotes growth and secretion in human polycystic kidney epithelial cells. *Kidney Int*. 2004;66(3):964–73.
33. Cao Q, Yu J, Dhanasekaran SM, Kim JH, Mani RS, Tomlins SA, Mehra R, Laxman B, Cao X, Kleer CG, et al. Repression of E-cadherin by the polycomb group protein EZH2 in cancer. *Oncogene*. 2008;27(58):7274–84.
34. Du J, Li L, Ou Z, Kong C, Zhang Y, Dong Z, Zhu S, Jiang H, Shao Z, Huang B, et al. FOXC1, a target of polycomb, inhibits metastasis of breast cancer cells. *Breast Cancer Res Treat*. 2012;131(1):65–73.
35. Vire E, Brenner C, Deplus R, Blanchon L, Fraga M, Didelot C, Morey L, Van Eynde A, Bernard D, Vanderwinden JM, et al. The polycomb group protein EZH2 directly controls DNA methylation. *Nature*. 2006;439(7078):871–4.
36. Mirzaei S, Gholami MH, Hushmandi K, Hshemi F, Zabolian A, Canadas I, Zarabi A, Nabavi N, Aref AR, Crea F, et al. The long and short non-coding RNAs modulating EZH2 signaling in cancer. *J Hematol Oncol*. 2022;15(1):18.
37. Dasgupta M, Dermawan JK, Willard B, Stark GR. STAT3-driven transcription depends upon the dimethylation of K49 by EZH2. *Proc Natl Acad Sci U S A*. 2015;112(13):3985–90.
38. Zhang X, Huang Y, Shi X. Emerging roles of lysine methylation on non-histone proteins. *Cell Mol Life Sci*. 2015;72(22):4257–72.
39. Jung HY, Jun S, Lee M, Kim HC, Wang X, Ji H, McCrea PD, Park JJ. PAF and EZH2 induce Wnt/beta-catenin signaling hyperactivation. *Mol Cell*. 2013;52(2):193–205.
40. Kim KH, Roberts CW. Targeting EZH2 in cancer. *Nat Med*. 2016;22(2):128–34.
41. Xu J, Wang Z, Lu W, Jiang H, Lu J, Qiu J, Ye G. EZH2 promotes gastric cancer cells proliferation by repressing p21 expression. *Pathol Res Pract*. 2019;215(6):152374.
42. Fan T, Jiang S, Chung N, Alikhan A, Ni C, Lee CC, Hornyak TJ. EZH2-dependent suppression of a cellular senescence phenotype in melanoma cells by inhibition of p21/CDKN1A expression. *Mol Cancer Res*. 2011;9(4):418–29.
43. Lee EJ, Seo E, Kim JW, Nam SA, Lee JY, Jun J, Oh S, Park M, Jho EH, Yoo KH, et al. TAZ/Wnt-beta-catenin/c-MYC axis regulates cystogenesis in polycystic kidney disease. *Proc Natl Acad Sci U S A*. 2020;117(46):29001–12.
44. Ghobashi AH, Vuong TT, Kimani JW, Ladaika CA, Hollenhorst PC, O'Hagan HM. Activation of AKT induces EZH2-mediated beta-catenin trimethylation in colorectal cancer. *iScience*. 2023;26(9):107630.
45. Zhang X, Li LX, Ding H, Torres VE, Yu C, Li X. Ferroptosis promotes cyst growth in autosomal Dominant polycystic kidney Disease Mouse models. *J Am Soc Nephrol*. 2021;32(11):2759–76.
46. Yan X, Xia Y, Li B, Ye Z, Li L, Yuan T, Song B, Yu W, Rao T, Ning J, et al. The SOX4/EZH2/SLC7A11 signaling axis mediates ferroptosis in calcium oxalate crystal deposition-induced kidney injury. *J Translational Med*. 2024;22(1):9.
47. Huang J, Zhang J, Guo Z, Li C, Tan Z, Wang J, Yang J, Xue L. Easy or not-the advances of EZH2 in regulating T cell development, differentiation, and activation in Antitumor Immunity. *Front Immunol*. 2021;12:741302.
48. Knutson SK, Wigle TJ, Warholc NM, Sneeringer CJ, Allain CJ, Klaus CR, Sacks JD, Raimondi A, Majer CR, Song J, et al. A selective inhibitor of EZH2 blocks H3K27 methylation and kills mutant lymphoma cells. *Nat Chem Biol*. 2012;8(11):890–6.
49. Guo Y, Cheng R, Wang Y, Gonzalez ME, Zhang H, Liu Y, Kleer CG, Xue L. Regulation of EZH2 protein stability: new mechanisms, roles in tumorigenesis, and roads to the clinic. *EBioMedicine*. 2024;100:104972.

Publisher's note

Springer Nature remains neutral with regard to jurisdictional claims in published maps and institutional affiliations.